Review Article

The potential of plasma-derived hard carbon for sodium-ion batteries

Abdul Wasy Zia [a,*], Shahid Rasul [b], Muhammad Asim [c], Yarjan Abdul Samad [d], Rana Abdul Shakoor [e], Tariq Masood [f]

[a] *Institute of Mechanical, Process, and Energy Engineering (IMPEE), School of Engineering and Physical Sciences, Heriot-Watt University, Edinburgh EH14 4AS, United Kingdom*
[b] *Faculty of Engineering and Environment, Northumbria University, Newcastle Upon Tyne NE1 8ST, United Kingdom*
[c] *School of Professional Education & Executive Development, The Hong Kong Polytechnic University, Kowloon 100077, Hong Kong, China*
[d] *Department of Aerospace Engineering, Khalifa University of Science and Technology, Abu Dhabi, United Arab Emirates*
[e] *Center for Advanced Materials, Qatar University, Doha 2713, Qatar*
[f] *Department of Design, Manufacturing and Engineering Management, University of Strathclyde, Glasgow G1 1XJ, United Kingdom*

A B S T R A C T

Sodium-ion batteries (SIB) are receiving wider attention due to sodium abundance and lower cost. The application of hard carbon to SIB electrodes has shown their significant potential to increase rates, capacities, stability, and overall performance. This article describes the significance of hard carbon, its structural models, and mechanisms for SIB applications. Further, this work unveils the potential of plasma methods as a scalable and sustainable manufacturing source of hard carbon to meet its increasing industrial demands for energy storage applications. The working mechanisms of major plasma technologies, the influence of their parameters on carbon structure, and their suitability for SIB applications are described. This work summarises the performance of emerging plasma-driven hard carbon solutions for SIB, including extreme environments, and revolves around the flexibilities offered by plasma methods in a wider spectrum such as multi-materials doping, in-situ multilayer fabrication, and a broad range of formulations and environments to deposit hard carbon-based electrodes for superior SIB performance. It is conceived the challenges around the stable interface, capacity fading, and uplifting SIB capacities and rates at higher voltage are currently being researched, Whereas, the development of real-time monitoring and robust diagnostic tools for SIB are new horizons. This work proposes a data-driven framework for plasma-driven hard carbon to make high-performance energy storage batteries.

1. Introduction

New and innovative energy storage solutions are evolving with NetZero global drive. Sodium-ion batteries (SIB) are receiving widespread popularity and being considered as a successor to lithium-ion batteries (LIB). Sodium (Na) has an ionic radius of 1.02 A°, is quite an abundant element with a concentration of 23,000 ppm, and has a carbonate cost of ~ £160 per tonne [1]. Whereas, the ion size, abundance, and carbonate cost of lithium (Li) are 0.76 A°, 20 ppm, and £4750 per tonne, respectively [2]. Academically, the number of scientific publications on carbon materials for SIB has reached beyond 1000 per year in recent years [3] along with their industrial embrace. SIB usually holds lower energy storage capacities than LIB, hence it struggled for more than two decades [4] with original equipment manufacturer (OEM) and suppliers for its commercialization. However, their applications are now

expanding beyond stationary energy storage units, particularly for five-passenger mid-range (257–450 km) electrical vehicles [1]. Capital research investments like the 2023 seed funding call of the Ayrton Challenge on Energy Storage (part of £1 billion Ayrton Fund by the UK Government) and, the NEXGENNA project funded by The Faraday institution, UK, are specifically boosting hard carbon research for SIB.

The carbon layers are perceived to prevent side reactions [5] and have shown their superior performance for SIB with retention capacities of 97 % and a prolonged lifespan of above 1500 cycles [6]. Particularly, hard carbon is being perceived as a promising candidate for SIB anode applications. This carbon allotrope is neither fully crystalline nor fully amorphous, but a mixture of rumpled and buckled graphenic sheets [7]. Hard carbon offers high conductivity of ions and electrons, structural stability, high capacity, lower working voltage, and low cost [8]. The European Commission report [9] has shown an attractive comparison of

---

* Corresponding author.
E-mail address: a.zia@hw.ac.uk (A.W. Zia).

hard carbon-based SIB with Lithium iron phosphate (LFP) batteries for energy density, cyclic durability, cost, and safety. The hard carbon based SIB was conceived as safer to transport than LIB; fast charging to 80 % state of charge in 15 min; cell cost was estimated at £0.036/Wh against £0.052/Wh for LFP; energy density in the range of 100 to 150 Wh/kg when compared to LFP range of 120 to 180 Wh/kg; capacity retention higher than 90 % at −20 °C which remains lower than 70 % for LFP; the cycle stability of above 2000 which more than 3000 for LFP. Commercial hard carbon based SIB cells launched in 2021 have shown higher energy densities of 160 Wh/kg with a potential of up to 200 Wh/kg and extraordinary cyclic stability of 12,000 cycles.

Mostly, the hard carbon for SIB is derived from numerous sources such as biomass [10], resin carbon [11] bio-waste [12], and organics [13] including, plants [14], cellulose [15], cedarwood Bark [16], Jute-Fiber [17], algae [18], pyroprotein [19] etc. The organic resources may have some limitations around commercial scalability as the hard carbon structure usually forms via specialized methods, such as pyrolysis, and interplanar distance between graphenic sheets is modulated [13] at high temperatures beyond 1000 °C [2,20]. Plasma techniques are emerging as a commercially viable candidate for the materials processing of SIB anodes. The hard carbon made through pyrolysis often needs post-processing to increase heterogeneity, disorder, and defective carbon entities. The microwaving process has shown the elevating capacity and rate capability of typical hard carbon. A short microwave treatment of only 6 s is demonstrated to uplift the reversible capacity of hard carbon from 204 to 308 mAh/g for SIB applications [21]. Spark plasma sintering has emerged [22] as a potential candidate to deposit hard carbon for SIB anodes with high throughput. The hard carbon produced with spark plasma sintering has shown better performance for SIB batteries due to higher conductance and lower oxygen contents achieved in rapid pyrolysis which are contrary to the typical methods. The preliminary proof-of-concept studies have demonstrated superior initial Coulombic efficiency (ICE) of 88.9 % with a rate capacity of 136.6 mAh/g at 5 A/g, and the reversible capacity of 299.4 mAh/g.

This work describes the mechanism of hard carbon for SIB application, hard carbon atomic models reported in history to the latest computational methodologies to study atomistic behavior to improve structure-property relationship for SIB anodes. An atomistic structure, variation in carbon sp^2 and sp^3 proportions, and disorder in hard carbon produced with plasma techniques are explained. Common plasma deposition i.e., physical vapor deposition (PVD), plasma enhanced chemical vapor deposition (PECVD) and low-pressure or atmospheric plasma deposition mechanisms and their suitability for SIB application are discussed. The emergence of core plasma techniques for Na-based batteries in order to uplift their capacities, stability and cycle life are reviewed. The last section highlights the current research challenges, ongoing aspirations and a digital manufacturing framework to make next-generation plasma-derived hard carbon SIB.

2. Mechanism of hard carbon for sodium-ion batteries

Hard carbon is getting recognition these years for SIB. The Coulombic efficiency of Na^+ batteries depends on the interplay of Na ions leaving and returning to the electrode and could be formulated as Eq. (1) [23].

$$\text{Coulombic Efficiency} = \frac{Discharge\ capacity}{Charge\ capacity}$$
$$= \frac{No.of\ Na^+ return\ to\ cathode}{No.of\ Na^+\ ions\ leaving\ cathode} \quad (1)$$

Fig. 1 presents the hard carbon structure and corresponding Na^+ mechanisms for SIB. The atomic bonding and microstructure of hard carbon significantly drive the overall battery performance. The efficiency of SIB depends on various factors such as surface area, surface energy, interplanar distance in graphitic sheets, number of vacancies and defects, porosity, active sites, and the pathway for the mobility of Na^+. Fig. 1 presents the known mechanisms of SIB by absorption, insertion, and pore/cavity filling of hard carbon. The **adsorption** of Na^+ occurs on active sites of the available surface area of hard carbon, which is normally the defects, vacancies, edges and active spots on the exterior of surfaces or the accessible area via open pores, cavities, and tunnels. The absorption in a pore and cavities is irreversible storage capacity. Adsorption of Na^+ overall influences the sloping region capacity of SIB. The **insertion** mechanism covers the penetration and mobility of Na^+ between graphene layers. Various models are reported in the literature advising recommended interplanar distance for Na ions and graphene sheets. Depending on insertion behavior, it impacts sloping and plateau capacities. The sloping capacity is affected by the random insertion of Na^+ among graphene layers with broad energy distributions, whereas the plateau capacity is influenced by procedural intercalation among graphene layers. Whereas, a **pore-filling** mechanism is attributed to the clustering of Na^+ in cavities and pores and their dimensional aspects. The pore-filling mechanism also impacts the plateau capacity of SIB. More details of Na^+ mechanisms for SIB are available in literature reports [24].

Fig. 2 presents the details of Na^+ storage mechanisms for SIB and how a storage mechanism or the combination of storage mechanisms impacts SIB storage capacities. It can be seen that current density and potentials are significantly boosted in adsorption-insertion hybrid mechanisms when compared to adsorption only.

3. Hard carbon models

3.1. Empirical models

There are continuous developments to illustrate hard carbon structures from history to the present era. Fig. 3A presents the developments
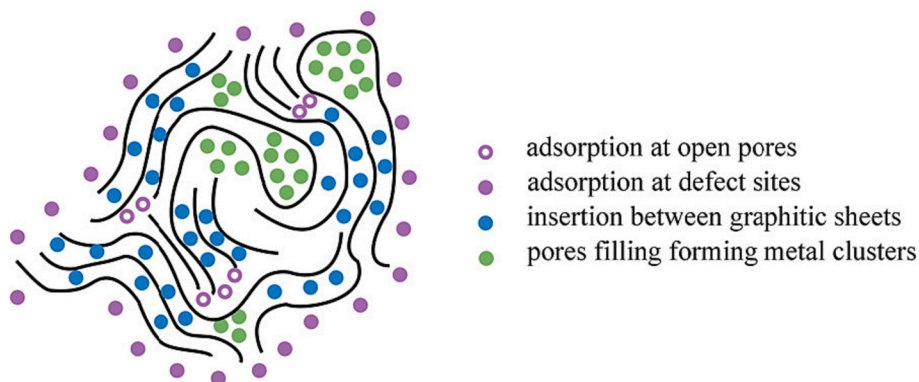

o adsorption at open pores
• adsorption at defect sites
• insertion between graphitic sheets
• pores filling forming metal clusters

Fig. 1. (A) Illustration of hard carbon structure and corresponding Na^+ storage mechanisms for sodium-ion batteries. Adapted from [24] CC BY, 2022, Wiley-VCH.
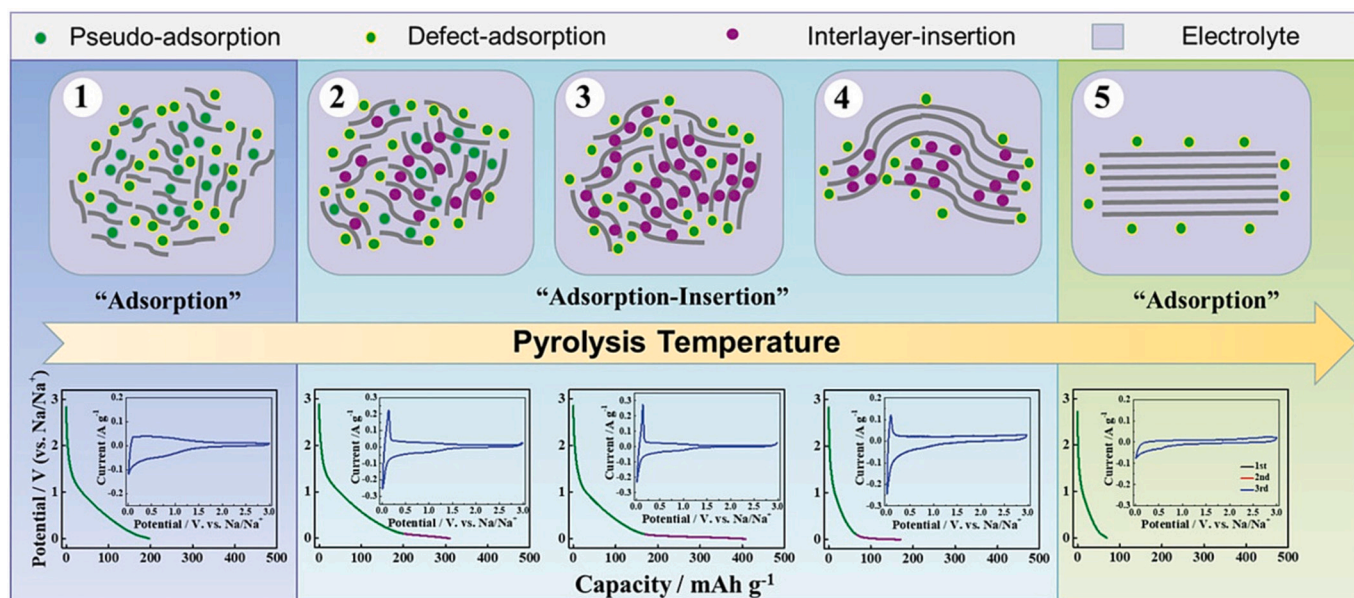
Fig. 2. The illustration of common Na$^+$ storage mechanisms and their potential vs capacity relationship as a function of pyrolysis temperatures. Reproduced with permission: Copyright 2019, Wiley-VCH [25]
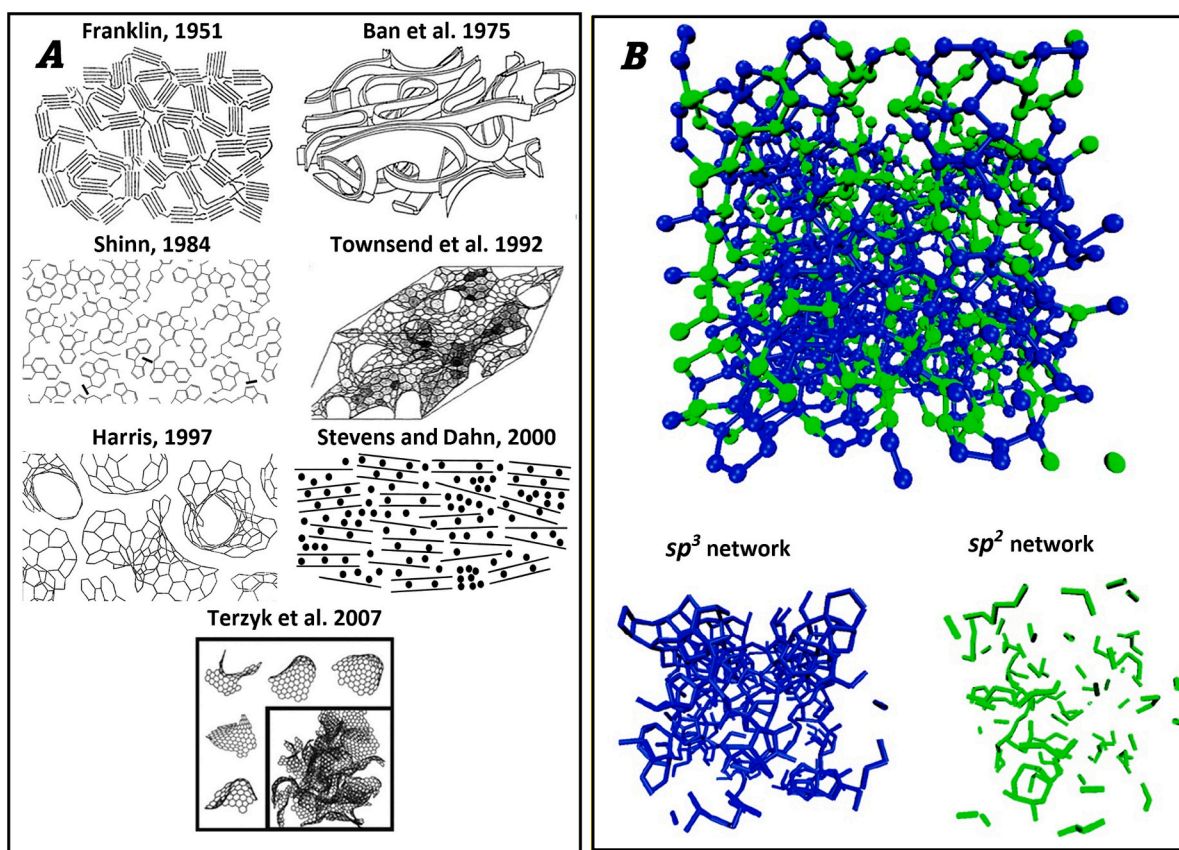

Fig. 3. (A) Major atomic structural models of hard carbon reported in history. Reproduced with permissions: Copyright 2019, Elsevier [28] and Royal Society of Chemistry [34]. (B) Molecular dynamics studies presenting overall atomistic structure and individual sp^2 and sp^3 carbon networks in plasma-derived amorphous carbon with a proportion of 71.3 % sp^3 bonds. Reproduced with permissions: Copyright 2015, Elsevier [33]. The authors of this work, Zia et al. propose hard carbon as a multi-scale disordered structure and suggest extending the definition from micro and mesoporous to atomistic levels.

in hard carbon models reported in the literature. Franklin [26] has presented a two-dimensional illustration of disorder crystallites/sheet bundles cross-linked with each other in random orientations. His work suggests formation of graphitizing and non-graphitizing carbon on thermal treatment between 1000 and 3000 °C. The density of graphitizing and non-graphitizing carbon and mean number of average layers

per parallel group increase with the increase in temperature. Further, the layer diameters reduce with increase in propotion of non-organized carbon. Likewise, the Shinn [27] model illustrates aromatic rings with several active sites, dangling bonds, and vacancies. His work originates from the coal liquefaction process and has identifies single-stage and two-stage structural products which differ in molecular weights, functionality, and stability. Steven and Dhan's [4] model is quite active these years and is known as "house of cards". It illustrates the accessible pathways of ions among sheets. Their work as claimed as first study demonstrating similarity between insertion mechanoms for sodium and lithium based on their model.

It is conceived that the hard carbon structure mostly includes twisted, rumpled, buckled graphemic sheets with various morphological features such as curves, bents, and non-planer orientations in three dimensions [28]. Hence, various three-dimensional models (Ban et al. [29], Townsend et al. [30], Harris and Tsang [31], and Terzyk et al. [32]) have attempted to reflect such features in their illustrations. Ben et al. [29] has performed imagining of non-graphitizing carbon which is heat treated from 529.85 to 2699.85 °C. Their work proposed a ribbon shaped structure based on their electron microscopy observations of intertwined crystallites which comprise of "*turbostratically packed aggregates of graphitic basal planes*". Townsend et al. [30] have performed computational modelling and generated various grapahtic structures with defined number of carbon rings. Their studies have found that the random structures are exceptionally stable when compared with periodic ones. Likewise, Terzyk et al. [32] model has explored non-graphitizing carbon through a group of fullerene-like, curved fragments randomly arranged together. Their work advance knowledge on pore size distributions and calculation of curved sp^2 sheets which do not contain hexagonal rings. Harris and Tsang [31] have also identified fullerene-like structure on heat treatment of non-graphitizing carbon between 2100 and 2600 °C. It could be deduced that all the models probably have attempted to highlight the presence of graphitic and non-graphitic structures, non-standard atomistic arrangements, porosity, defects, vacancies, dangling bonds, active sites, and accessible pathways which are likely to maximize the opportunities for ion storage and mobility.

This work extends the definition of hard carbon from micro and mesoporous to atomistic levels with an example of the plasma-derived amorphous carbon which is composed of disordered carbon atoms connected in the form of chains and rings and develop carbon sp^2 and sp^3 network with atomic scale porosities. Fig. 3B presents the molecular dynamics studies of plasma-derived carbon with 71 % sp^3 contents [33]. A highly disordered carbon structure can be observed either for combined or individual sp^2 and sp^3 carbon networks, thus, the availability of higher surface area, number of active sites and dangling bonds, and atomic scale porosity make it a high potential candidate for superior electrochemistry of elements with comparable atomic/ionic sizes.

3.2. Computational models

Application of computational tools on hard carbon for SIB including physics-based modelling [35], first-principles studies [36,37], image processing [38,39], density-functional theory and molecular dynamics [40], and machine learning [41] taking hard carbon studies to new horizons by developing atomistic understanding. A physics-based pseudo-two-dimensional [35] model of hard carbon for SIB anode has shown high accuracy in predicting discharge profiles. This model used genetic algorithm and experimental data to perform rapid parametric optimization and is aspirant to do multi-objective optimizations by including cell design, electrode material and dimensional features, and cost etc. First-principles calculations based on joint density functional theory using 'nonlinear polarizable continuum model' and 'Charge-asymmetric nonlocally-determined local electric solvation model' suggests preferred sites for adsorption which are mono-vacancy, di-vacancy, and Stone-Wales due to implicit interaction in hard carbon for SIB

application [37]. Similarly, first-principles calculations using joint density functional theory, nonlinear polarizable continuum model and pseudopotential atomic orbital method have investigated the armchair and zigzag edge parameters to understand the charge transfer mechanisms and energy profiles with solvents in aspiration to optimize electrolyte for SIB [36]. Similarly, the density functional theory and Monte Carlo simulations are used to discover new materials and formulations. Those computational studies have suggested T- Carbon as a potential element for battery anodes. The T-carbon exhibits a diamond phase with an acetylene bond in a hollow structure [42] and has good potential for SIB batteries. Referring to image processing techniques, an image-guided construction study of hard carbon gives the atomistic structural representation, where the algorithm automatically calculates the interlayer spacings. This digital development helped to understand the structure-property relationship and is considered a pathway to fabricate high-performance hard carbon anodes for SIB [38]. Likewise, intelligent image analysis frameworks are being developed to analyse hard carbon morphologies with fringe analysis and Gabor filtering algorithm for robust fetching of accurate, meaningful, and reliable data to understand the property-structure relationship of hard carbon for SIB [39].

Fig. 4 presents the molecular dynamics studies [43] of carbon that reflects a relationship between atomic density and sp^3 network. The blue and red dot corresponds to carbon sp^2 and sp^3 atoms, respectively. Referring to 4 A, the sp^3 amounts of 12.5 %, 59 % and 76 % correspond to the density of 2.10 g/cm^3, 2.88 g/cm^3, and 3.31 g/cm^3, respectively. Likewise, Fig. 4B also suggests that the density of carbon proportionally increases with sp^3 fraction. Another molecular dynamics study [44] of DLC made with carbon ion energies of 1 eV and 70 eV which correspondingly influence their sp^2 and sp^3 compositions and porosity. For mechanical applications, 70 eV energy is desirous as DLC aimed to have the highest possible sp^3 phase and density which uplifts overall hardness and tribological performance. However, a much higher density may hinder sodium mobility for sodium battery applications. A recent study suggests that there are about ~40 % surface defects in tetrahedral carbon [45]. Such surface defects, porosities and tunnels are essentially required for sodium ion mobility in SIB applications. Hence, there is a need to investigate the optimum amount of surface defects and porosities required for superior SIB performance. Therefore, plasma-based carbon needs to be revisited for scientific mechanisms, process-property-performance relationships, and limitations specifically in the context of sodium battery applications.

Fig. 5A presents the range of atomic environments forecasted through computational methods after validation of experimental data. Depending on precursors, synthesis methods and experimental conditions, hard carbon could have different atomistic patterns such as hexagonal rings, 3, 5 and 7 membered rings, edge sites, pores, methyl and methylene sites, sp^2 and sp^3 bonds. Fig. 5B presents the sodium mapping of 8000 samples to reflect their binding distribution with hard carbon. The image is superimposed with distribution of sodium sites in hard carbon across surfaces, crease, and interlayer. It is conceived that that sodium attach at continuous of void volume; in lines with crease of folds and bends; and at interlayer sites where sheets or structures are pitched together. More details are available in the literature report [46].

3.3. Data-driven approach for modelling

Machine learning is emerging to reveal hard carbon atomistic behaviours for SIB batteries. A combination of machine learning and density functional theory has demonstrated Na intercalation behaviours for disorder carbon [40]. Machine learning tools are used to optimize structural parameters (interlayer spacing d_{002}, a-axis L_a, and the c-axis L_c) of disordered carbon having a vital potential to give higher ICE, capacity and working plateau for SIB batteries [41]. Further, a standardization process was proposed [41], as shown in Fig. 6, which suggests standardizing structure-property data such as the data obtained from Raman spectroscopy, X-ray crystallography, BET (Brunauer,
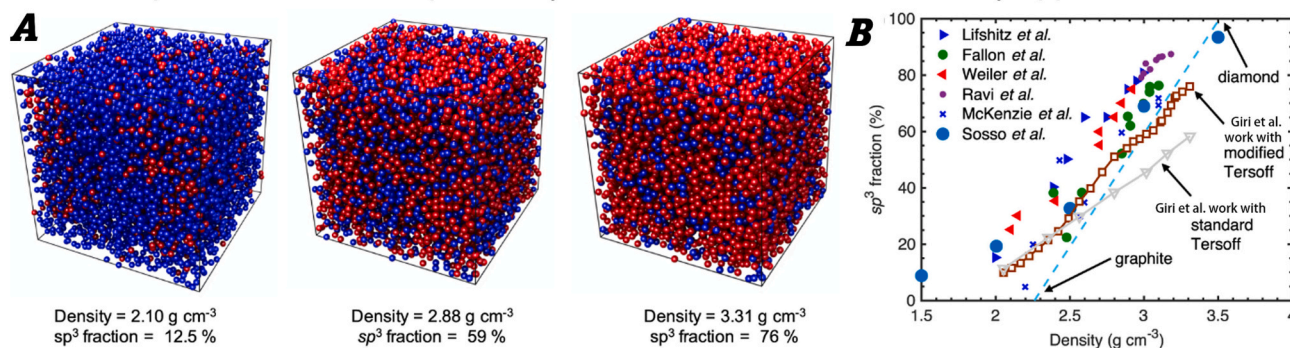
Fig. 4. The atomistic structure of carbon virtually deposited through molecular dynamics simulations presenting a relationship between sp^3 proportion and density of plasma-derived carbon.
Adapted from [43], CC BY, Springer Nature.
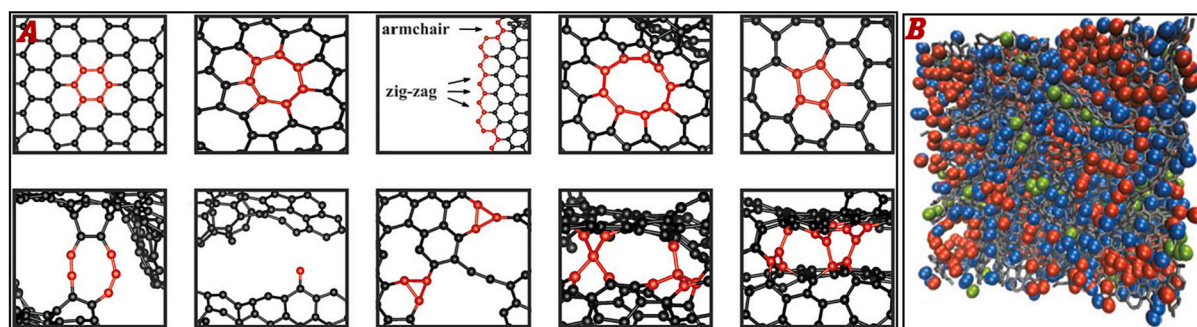
Fig. 5. (A) Range of atomistic arrangements and (B) superimposed sodium locality at surfaces (red circles), crease (blue circles) and interlayer (green circles) in hard carbon studied with computational tools. (For interpretation of the references to colour in this figure legend, the reader is referred to the web version of this article.)
Reproduced with permissions: Copyright 2022, WILEY [46].
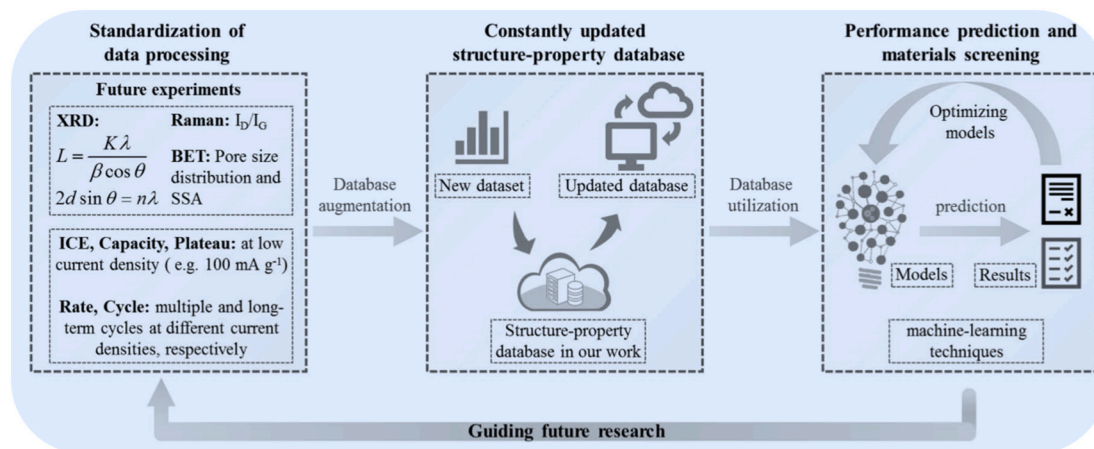
Fig. 6. A standardization framework for disorder carbon materials on structure-property data structuring, continuous updating of the database, and screening optimum parameters using machine learning tools.
Reproduced with permissions: Copyright 2022, The Royal Society of Chemistry [41].

Emmett and Teller) etc. and corresponding ICE, capacities, plateau, rate and cycles. The standardised data will lead to the formation of a structured database that can be continuously updated. Further, the machine learning-based optimization and predictive models will process the data to suggest best parameters to develop high-performance hard carbon anodes for SIB.

4. Plasma derived hard carbon

Typically, the carbon is applied on SIB anodes by mechanical mixing [47] and followed by high-temperature pyrolysis. However, the plasma-based deposition of carbon has delivered superior performance for LIB and has vital potential for SIB considering quality, scalability, and cost. The following sections dedicatedly describe the structure and deposition methodologies of plasma-based carbon and their suitability for SIB.

4.1. Structure of plasma derived hard carbon

Plasma technologies are well-recognized to deposit a variety of carbons such as diamond-like, graphite-like, amorphous, nanocrystalline, granular, etc. PVD and PECVD have a history of producing carbon layers and their superior performance for LIB has been investigated with size, thickness [48], coverage, and morphology [49] factors in past years. The plasma-based hard carbon solutions are now emerging for SIB. In preliminary studies, hard carbon derived from spark plasma sintering has shown a superior initial coulomb efficiency of 88.9 % [50].

The synthesis of hard carbon via plasma methods and its performance for SIB are governed by the composition of carbon sp^2 and sp^3 phases in the hard carbon. Fig. 7 explains how the sp^2 and sp^3 composition influence the production of hard or soft carbons. Referring to Fig. 7A, the ternary diagram shows the mapping of various types of carbon or hydrogenated carbon structures. The ternary diagram presents the atomic arrangements of carbon atoms in diamond (100 % sp^3), graphite (100 % sp^2) and hard carbon (mixture of sp^2 and sp^3) material. The diamond is composed of a tetrahedral structure where every carbon atom develops covalent bonding with four surrounding carbon atoms. While the carbon atoms arrange themselves into an aromatic ring and make covalent bonds with adjacent carbon atoms within the same plane for graphite. Whereas in the case of hard carbon, an engineered carbon structure, is highly disordered and a mixture of sp^2 and sp^3 bonds where sp^2 atomic clusters are bonded to sp^3 networks. The structure is often recognized as diamond-like with a higher sp^3 phase and graphite-like or polymeric carbon [51] with a higher sp^2 phase, respectively. There is no precise location of diamond-like carbon (DLC) structure within a ternary
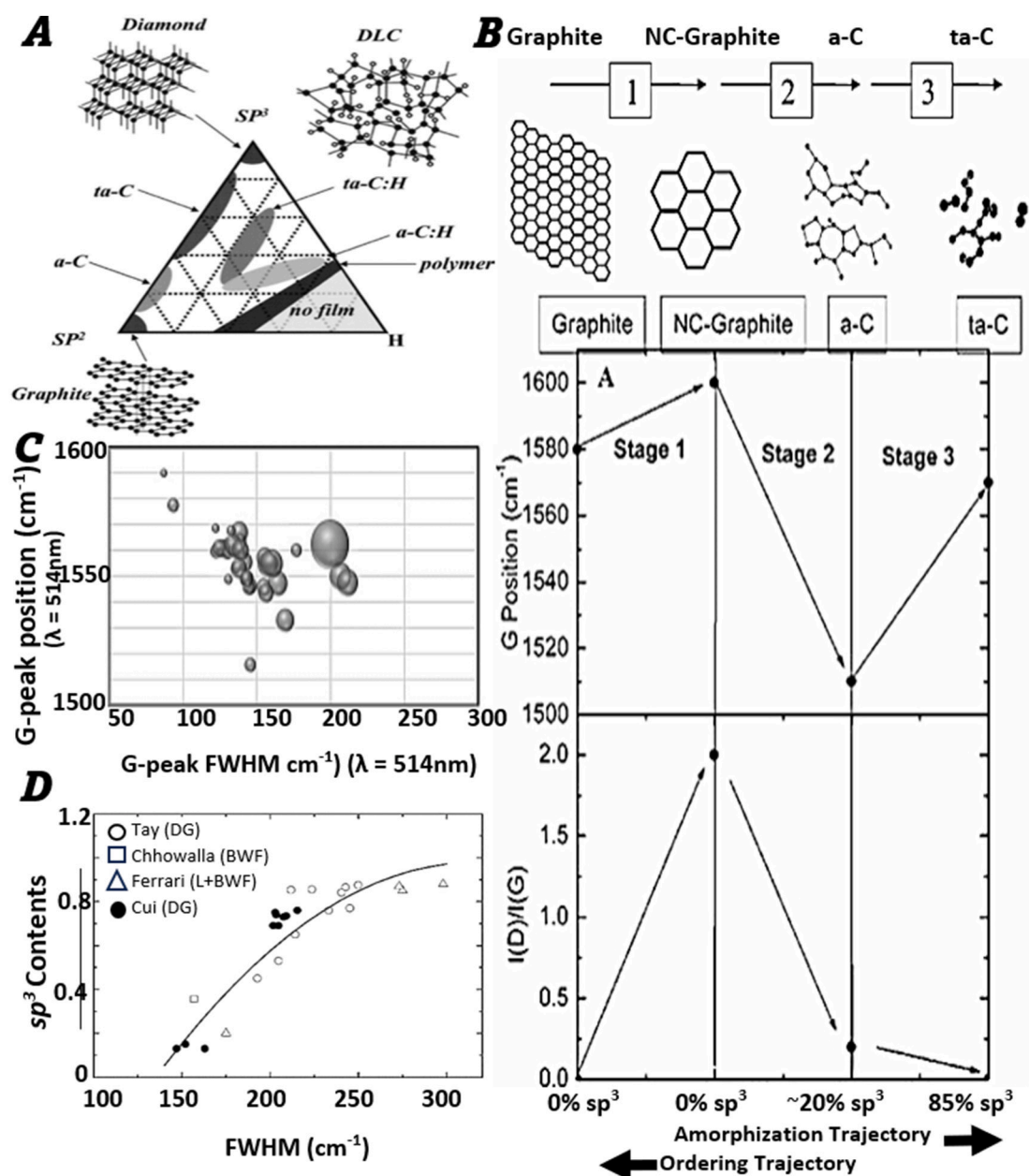
Fig. 7. (A) Ternary diagram of carbon structures on the bases of sp² and sp³ compositions and hydrogenated and non-hydrogenated carbon types. Reproduced with permissions: Copyright 2017, KOBELCO, Japan [54]. (B) Ferrari Three-stage model correlation carbon structure and Raman spectra information (IG peak positions, ID/IG) as a function of sp³ contents. Reproduced with permissions: Copyrights 2003, American Physical Society [53]. (C) Relationship between IG peak position FHWM for carbon structure, suggesting highest disorder against Raman shift of 1550 ± 10 cm⁻¹. Reproduced from CC 4.02021, MDPI [55]. (D) A relationship between sp³ vs FWHM suggests that the sp³ bonds increased with carbon disorder in layer. Reproduced with permissions: Copyright 2010, Elsevier 2010 [56].

diagram but generally, it is the central zone of ternary diagram [52] relatively closer to sp^2 - sp^3 element. The transition between graphite-like and diamond-like structure occurs with the transformation of amorphous carbon (a-C) from aromatic rings into carbon chains developing a tetrahedral carbon (ta-C) structure as mapped in ternary diagram (Fig. 7A) and depicted in Fig. 7B. The PVD and PECVD methods used to make these diamond-like hard carbon are detailed in Section 4.2.

Fig. 7B is a Ferrari three-stage model [53] that correlates the carbon structure and Raman information as a function of sp^3 percentage. The level of disorder in hard carbon is qualitatively assessed with their IG peak positions and FWHM values. The graphitic materials mark their IG position between the Raman shift of 1580 and 1600 cm^{-1}. The a-C (ring structure) usually has a 20 % sp^3 bond and the ta-C (chain structure) has sp^3 bonds up to 85 % marking the IG peak position at the Raman shift of 1520 cm^{-1} and 1570 cm^{-1}, respectively. The diamond-like hard carbon structure (as depicted in Fig. 7A), a highly disordered mixture of ring and chain structure marks IG values between 1540 cm and 1560 cm^{-1}. The ID/IG proportions change with a carbon structure, accordingly. Likewise, the crystalline materials show a sharp narrow peak at a certain Raman wavelength, such as diamond at 1332 cm^{-1}, silicon at 5,20 cm^{-1} and graphite around 1600 cm^{-1}. Hence, narrow Raman peaks correspond to small FWHM values while the broader peaks give higher FWHM values and reflect a proportional increase in structural disorder. Fig. 7C presents that the FWHM of diamond-like hard carbon structure is highest at Raman shift of 1550 $\pm$ 10 cm^{-1} where the highest disorder could be expected due to a mixture of ring and chain structures. Likewise, Fig. 7D presents the direct relationship of FWHM vs sp^3 contents which suggests that the increasing disorder ensures a higher number of sp^3 bonds. The high disorder in carbon atoms and higher number of sp^3 bonds maximize the chances of Na$^+$ adsorption, insertion, and pore-filling mechanism to enhance the overall performance of SIB batteries.

Fig. 8A presents the HRTEM atomic mapping of free-standing monolayer carbon. The images are processed for better visualization and identification of compositions such as pentagons in red colour, heptagons and octagons in blue colours, and hexagons in purple colour and green colour is used for crystallites. Fig. 8B presents the zoomed-in image of the red square in Fig. 8A. The mixture of carbon rings and varying angles among each ring reflect the disorder of structure in a two-dimensional plane. Fig. 8C presents ReaxFF Molecular dynamics studies of hard diamond-like carbon structure in three dimensions with a density of 3240 Kg/m^3 and cross-validated with XAES experimental studies. It presents the tetrahedral network of 71.5 % sp^3 bonded carbon atoms (red), 28.1 % sp^2 bonds (blue) and 0.4 % of sp^1 bonds (green). The sp^1 bonds are unstable with the shortest lifespan. Along with highly disordered networks of carbon atoms, it can be observed that the atomic bonding composition varies from bulk to surface or vice versa. The sp^1, sp^2 and sp^3 proportions are 11 %, 37 %, and 52 % at the surface while 0 %, 32 %, and 68 % within the bulk. Fig. 8D presents the MD simulation of hydrogenated hard carbon [57,58]. The attachment of hydrogen atoms to the dangling bonds reflects the enriched availability of active sites and anticipates a higher potential for Na$^+$ to develop similar mechanisms for SIB applications. Fig. 8E and Fig. 8F are a detailed visualization of Fig. 8C and separately present a tetrahedral network of 71.5 % sp^3 bonds (Fig. 8E) and sp^1 and sp^2 bonds (Fig. 8F) in 3180 Kg/m^3 dense hard carbon.

4.2. Manufacturing of plasma derived hard carbon

The empirical [61] and experimental [62] studies suggest that the optimum ion energy of 100 eV gives the highest sp^3 proportion in carbon films [63] when made through plasma methods. Fig. 8 gives an overview of three major plasma deposition groups to make hard carbon for SIB anodes. The plasma deposition groups work on varying principles and, therefore, produce carbon species of different kinetic energies.

4.2.1. Physical vapor deposition (PVD) technology

Physical vapor deposition (PVD) mainly includes sputtering, evaporation, arc discharge, and numerous types of ions, electrons, and laser beam methods where the material to be deposited is transported from the solid carbon target and deposited at substrates to deposit a thin carbon layer.

4.2.1.1. Sputtering deposition.
Fig. 9A illustrates the fundamental sputtering process. In sputtering, the carbon atoms leave the target, get charged by receiving free electrons and ions, and grow into nano seeds by physical collusions and making chemical bonds due to electronegativity differences. The nano seeds pass through coalescence and clustering phases and arrive at substrate (i.e., the anode in the case of SIB) as atomic clusters by passing through seeding, coalescence, and clustering phases to deposit a thin film of hard carbon. More details on the growth mechanism could be found in the literature [64]. The carbon species usually have kinetic energies in the range of 2.5 to 25 eV [51] for sputtering depositions. The sputtering technology is sub-categorized as magnetron [65], direct-current [66], radio-frequency [67], balanced [68] and unbalanced [69] magnetron sputtering and some other variants [70] subjected to the type of electric power inputs and arrangements of magnetic fields. The corresponding nature of electrostatic potentials and magnetic fields influence the degree of ionization of carbon atoms, growth mechanism, deposition rates, density and porosity in carbon films. Usually, the sp^3 phase in carbon made with sputtering methods remains 50 % or lower unless made with specialized sputtering techniques [71].

4.2.1.2. Arc deposition.
The arc technology is well recognized for depositing carbon with higher sp^3 bonds. The sp^3 phase in hard carbon is often above 80 % when produced with arc systems [72,73]. The arc plasma is ignited by applying a high electric potential between electrodes. The carbon atoms usually have energies in the range of ten to several hundred [74] eV in arc discharge. There are two common categories in arc discharge deposition. The substrate is either directly exposed to arc discharge [75] or the plasma is transported [76] through C, S, and T-shaped ducts to a substrate as shown in Fig. 9B. The plasma density and transportation are regulated with the application of magnetic fields. The plasma ducts are made with single or double bends (C, S, and T shapes) to filter out unwanted microparticles. The yield rate and porosity are usually higher for direct depositions which are reduced in single and double-bend arc systems. Considering hard carbon requirements for SIB, the direct arc plasma discharge would be suitable to produce a hard carbon structure with high throughput and relatively more porosity. Whereas the single and double-bend cathodic arc systems have significantly lower deposition rates and are chosen in aspiration to make dense and defect-free carbon layer which is not desired for SIB batteries.

4.2.1.3. Ions, electrons and laser based depositions.
The carbon is also deposited with numerous types of energy beams, such as ion [77], electron [78], or laser beams [79]. Fig. 9C shows the deposition of thin film deposited with lasers as a representative example. Irrespective of type, the energy beam sputters the carbon atoms from the target which are then transported to a substrate in the form of atoms or ions to form a thin film. Although, pulsed laser deposition, ion beam and electron beam depositions are quite common to form a hard carbon. These methodologies may have limitations for SIB anode applications due to small-area deposition.
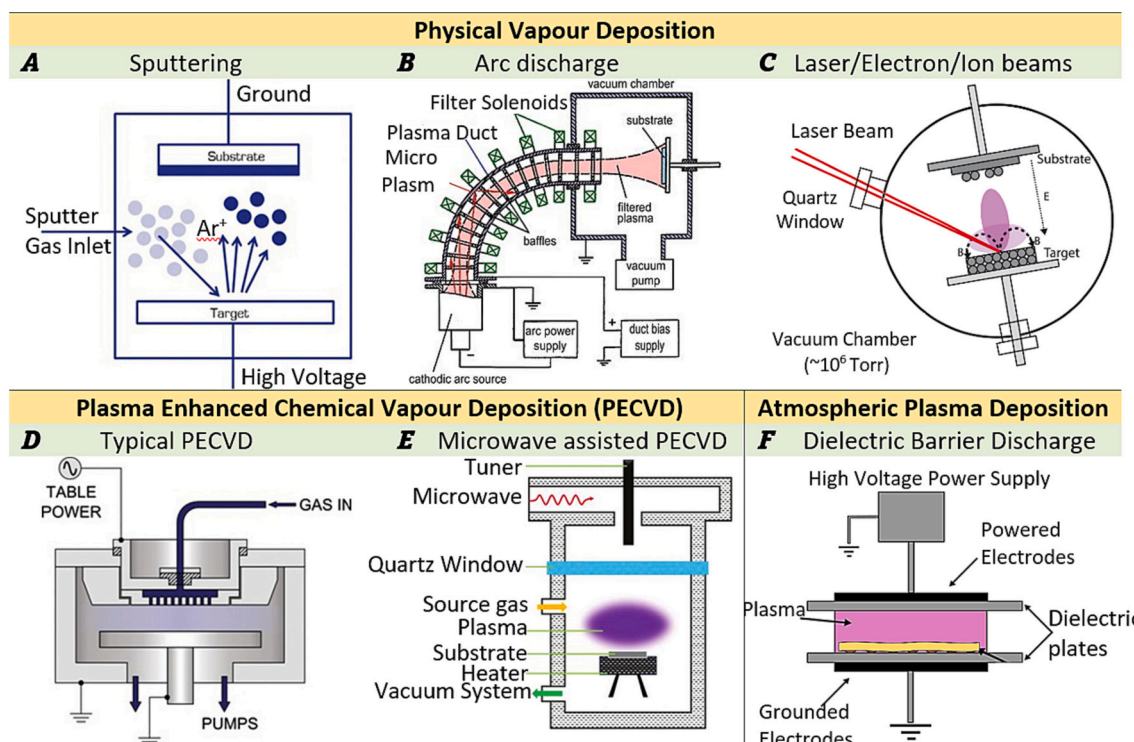
4.2.2. Plasma enhanced chemical vapor deposition (PECVD) technology

Contrary to solid carbon sources in PVD, the Plasma Enhanced Chemical Vapor deposition (PECVD) technique deposit a hard carbon layer from carbonous vapours formed by chemical reactions from gaseous precursors [80] in the presence of electrical and magnetic
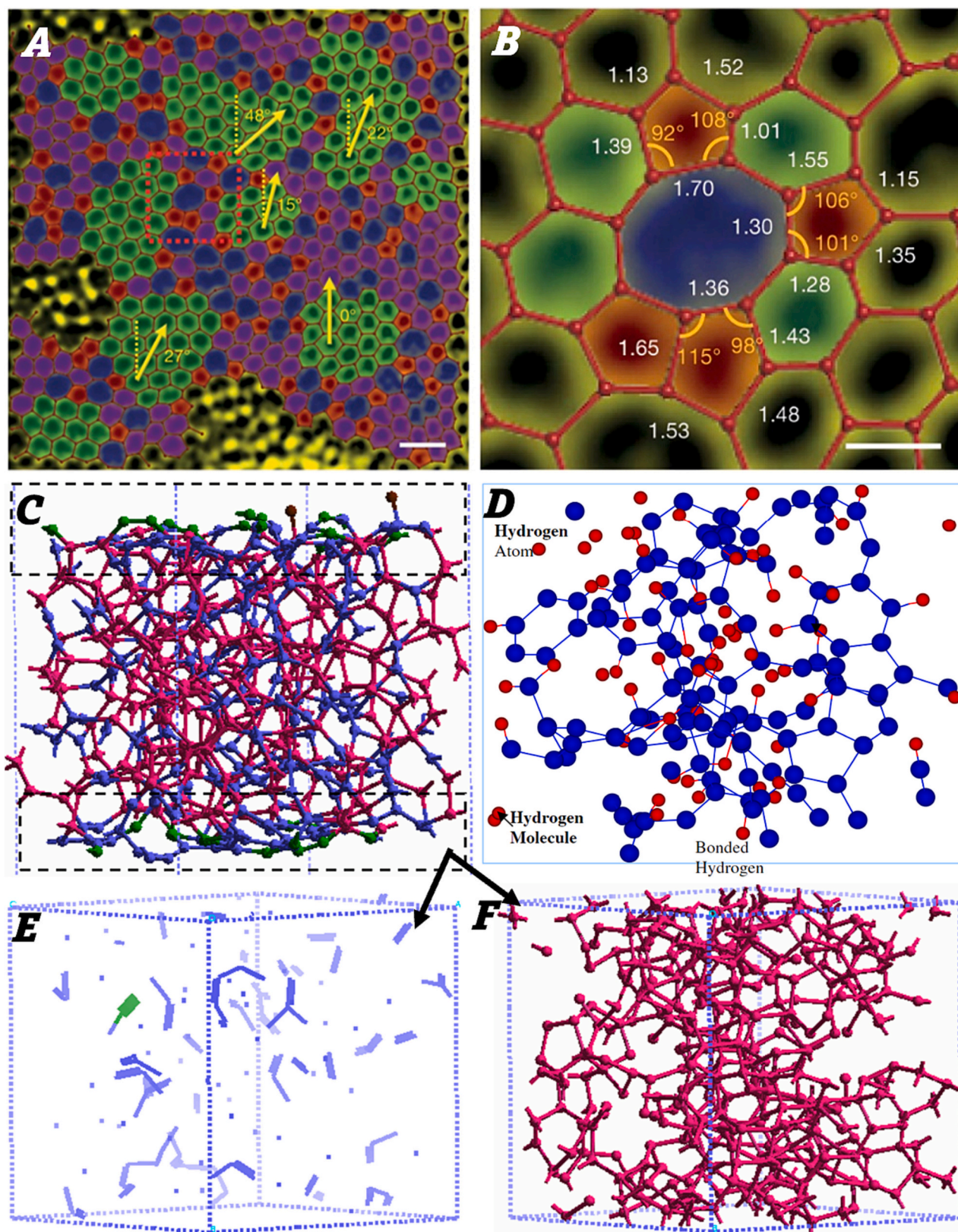
Fig. 8. (A) HRTEM and colour processing atomic mapping of free-standing monolayer carbon and (B) zoomed-in red square in (A) presenting disorder/mixture of carbon atomic structure in a two-dimensional plane. Reproduced with permissions: Copyright 2020, Springer Nature [59]. (C) ReaxFF Molecular dynamics of hard diamond-like carbon studies present a combined three-dimensional network of sp^2 and sp^3 carbon atoms. While (D) presents the atomic scale molecular structure of hydrogenated hard carbon (large circle presents carbon and small circles present hydrogen). Reproduced with permission, 2006, IOP Publishing [57]. (E) presents sp^2 and (F) presents sp^3 network of carbon atoms presented in (C). Fig. 6C, E and F reproduced from CC BY 2007, IOP Publishing [60]. (For interpretation of the references to colour in this figure legend, the reader is referred to the web version of this article.)

Fig. 9. Representative examples of Plasma Vapor Deposition methods such as (A) Sputtering, (B) Arc Discharge, (C) laser/electron/ion beams; Plasma Enhanced Chemical Vapor Deposition methods: (D) Typical PECVD deposition and (E) Microwave enhanced PECVD deposition; and Atmospheric Plasma Deposition family such as (F) Dielectric Barrier Discharge to deposit carbon layers.
Reproduced from A [90] B [91], C [92], D [90], E [93], and F [94].

potentials. Benzene, acetylene, cyclohexane are common examples of gaseous precursors that give higher deposition rates of hard carbon than methane and ethane [81]. Similar to PVD, the PECVD is also sub-categorized based on radio-frequency, alternating current, direct current, microwave plasma etc. Fig. 9D and E show representative examples of alternating current and microwave plasma based PECVD reactors. Each method varies in mechanism and provides certain levels of dissociation energy to carbon precursors. The above-described methane, ethane, cyclohexane acetylene, and Benzene correspond to ionization potential (eV) of ~ 12.4, ~ 11.4, ~ 9.8, ~ 9.3, and ~ 9.25, respectively [81]. Hence, different precursor needs a different level of energy inputs to produce carbon species with 100 eV ion energies. Similarly, the hard carbon density also depends on the electrostatic potential provided to the substrate [82]. The PECVD methods can offer more flexibility for hard carbon SIB anodes in terms of secondary and tertiary doping, reactive synthesis, high-temperature deposition and post-thermal treatments.

4.2.3. Atmospheric plasma deposition technology

PVD and PECVD technologies require deposition of hard carbon under a high vacuum and some factors are also associated with high capital cost, confined scalability, product complexity, and prolonged process time. The atmospheric plasma deposition [83] family is swiftly growing these years to provide rapid, economical, and higher deposition rates of carbon. The plasma is produced between two electrodes and atmospheric plasma setups vary by radio frequency, alternating current, direct current, and microwave plasma types and ambient or aqueous environments. Micro-plasma [84], dielectric-barrier-discharge [85], electrolysis [86], plasma guns [87], plasma jets [88], and microwave resonators [89] are common atmospheric plasma deposition systems to deposit carbon. Fig. 9F shows the dielectric-barrier discharge as a representative example of the atmospheric plasma family. Normally, the atmospheric plasma reactors require small capital investment and are

custom-built and tabletop setups. The electrode designs and configuration provide tremendous flexibility to synthesise nanomaterials and functional layers specific to substrate morphologies. The array of electrodes promotes large-area deposition on scalability aspects.

Irrespective of the plasma deposition family, the deposition parameters greatly influence the characteristics and performance of hard carbon. Ion energy, ion flux, plasma frequency and density, electrostatic potentials, magnetic fields, thermal environments, vacuum levels in case of PVD/PECVD, process and reactive gas and their flow rates significantly modulate deposition rates, layer thickness, and mainly the amount of sp^3 bonds in hard carbon which govern their electrochemical performance. The process-structure-property relationships of plasma-derived carbon are available in the literature [81,95,96].

5. Emerging plasma-derived hard carbon solutions for sodium-ion batteries

Referring to plasma applications for sodium batteries, the oxygen plasma treatment of hard carbon for SIB is reported to turn hard carbon surfaces into a hydrophilic nature for better solid electrolyte interfacing [97]. The oxygen plasma processing has uplifted specific capacity from 225 to 325 mAh/g (44 % increase) at the current rate of 50 mA/g. Further, incorporating oxygen and nitrogen groups is anticipated to yield long-term cyclic performance [98]. Similarly, facile oxygen plasma process of hard carbon at room temperature, 30 MHz frequency and 300 W power [99]. The oxygen plasma processing has enhanced initial Coulombic efficiency from 60.6 % to 80.9 % (33 % increase) and also reflects the enrichment of Na$^+$ in active spaces after the addition of oxygen groups.

Similarly, the PECVD system is used to carbonize phenolic resin aerogel to develop integrative carbon network material [100]. The PECVD supported large-scale processing and assisted in regulating oxygen groups and carbon structure to boost rate and cycle capabilities. An

integrative carbon network-based anode made with the PECVD process has provided the reversible capacities of 101.9 mAh/g at 1000 mA/g. Further, the reversible capacities were retained at 76 % beyond 2000 cycles. Similarly, the nanostructured DLC deposited with RF sputtering have uplifted reversible capacity and output voltage of about 2.3 V when adopted for sodium air battery [101]. The carbon deposited with an electrochemical process and enhanced with ultrasonication and acid washing have shown reversible capacities of ~ 170 mAh/g at 10 mA after 50 cycles [102].

Referring to atmospheric plasma depositions, the hard carbon made with a spark plasma sintering process have shown ICE of 88.9 % and a reversible capacity of 299.4 mAh/g. Whereas, the rate capacity was 136.6 mAh/g at 5 A/g. The overall performance was better or matchable with typical SIB [22]. The rapid pyrolysis reactions during the spark plasma sintering process make hard carbon with lower oxygen contents and higher electronegativity, which improves the electrochemical performance of SIB. The preliminary studies have proven the potential of plasma-based carbon for SIBs and could be systematically investigated to reveal their maximum potential. Similarly, the solution plasma processing technique is demonstrated to prepare doped carbon for SIB anodes. The phosphorus doping in carbon produced with solution plasma processing [103] is perceived to create abundant active sites which promote Na ion functioning and has shown 75 % ICE and reversible capacity of 340 mAh/g at 1 A/g current density, respectively. The solution plasma processed phosphorus-doped carbon anodes have shown a reversible capacity of 83 mAh/g beyond 40,000 cycles. Further, the rate performance was 130 mA/g at a current density of 100 A/g. Another study also reported the synthesis of nitrogen and sulfur-doped carbon-based anode for a sodium-based secondary battery using one-step plasma in a liquid process and delivering 35,000 cycles at an ultra-high current density of 100 A/g [104].

6. Challenges and future aspects

Although hard carbon is fairly attractive for SIB but there are still opportunities to advance the performance and mechanisms, and to minimise the limitations i.e., change in morphology and volume during the sodium insertion/extraction process which limits the cycle life [105], capacity fading [106] etc. Generally, SIB relatively have lower capacities than LIB which needs to be uplifted to make it a strong competitor [107] and to extended its usability for heavy duty applications like power tools, aerospace etc. Various materials designs, architectures, additives, dopants, and formulations are being explored and aqueous and solid electrolytes [108,109] and interfaces are being designed to further improve hard carbon performance for SIB.

The plasma technologies have enriched capability to perform multi-material dopings and in-situ microstructure tailoring. The recent non-plasma developments in hard carbon solutions for SIB could be scalable for large-scale manufacturing using plasma technologies. Referring to the material doping, the hybrid framework of metal and carbon has shown a capacity of 72 mAh/g at a current density of 200 A/g and capacity retention of 90 % beyond 15,000 cycles at a current density of 5.0 A/g [110]. Similarly, double-coated hard carbon anodes have proven their performance for LIB with a reduction in first irreversibility from 24.3 to 8.1 % and specific surface area from 10.2 to 2.8 [111]. Similarly, various material designs and architectures are now emerging for SIB. A soft carbon layer on free-standing hard carbon has shown its potential in reducing oxygen-containing groups and therefore achieving ultra-high initial Coulombic efficiency of 94.1 % and stable cyclic performance as the capacity retains at 99 % beyond 100 cycles at a current density of 20 mA/g [112]. A multiscale micro-nano hard carbon structure derived from filter paper is reported to have a reversible capacity of 286 mAh/g at 20 mA/g beyond 100 cycles [113]. Similarly, the decoration of hard carbon with silicon nitride nanoparticles has shown regulating electrochemical reactions and demonstrated an increase in reversible capacity from 284 to 351 mAh/g [114]. The addition of zeolite and carbon black

[115] as ionic and electronic conducting additives to hard carbon has shown improving rate performance and ageing characteristics such as cyclic stability and lower Na plating. The zeolite nanomaterial reduces the solid-electrolyte interphase on hard carbon and facilitates Na^+ mobility. Similarly, sulfur, boron and phosphorus dopings into hard carbon have been investigated to modulate interlayer spacing to regulate low-potential plateau capacities [116].

Fig. 10 shows the plane (Fig. 10A) and cross-sectional (Fig. 10B) micrographs of a hybrid MXene and hard carbon film for SIB anodes. The incorporation [105] of MXene ($Ti_3C_2T_x$) with hard carbon films has been shown to promote a three-dimensional conductive network. Consequently, the new materials combination has delivered a high capacity of 346 mAh/g and remarkable stability beyond 1000 cycles. Fig. 10C, D, and E present the Cyclic-Voltammetry (CV) curves, the relationship between peak current and sweep rate, and diffusion/capacitive contributions as a function of scan rates for MXene and hard carbon hybrid films. Usually, CV relationships have similar profiles. The addition of MXenes into hard carbon has shown regulating insertion and release of Na^+ and pseudo-capacitance for CV profiles, a diffusion-controlled process for peak current and sweep rate relationship, and the significance of capacitive process for SIB. The addition of MXene is perceived as a binder to improve structural stability as well.

SIB performance in extreme weather is oncoming area. Hard carbon-based electrodes have shown their ability to perform at −40 °C [117]. The hard carbon in combination with perfluoropolyether electrolytes for SIB have shown excellent performance of 99.8 % Coulombic efficiency, stable rate capacities, and high current density of 80 mA/cm^2 [118]. Sodium dissolution at interphase is perceived as more intense than LIB and causes a reduction in stability and irreversible capacity, electrolyte depletion, and continuous side reactions. Hard carbon has been perceived as lowering the Coulombic efficiency in past 20 years due to the formation of a solid-state electrolyte interface layer [119]. However, recent studies have demonstrated improved capabilities to develop a stable interphase with capacity retention beyond 90 % after 300 cycles at 4.2 V [120]. Hard carbon-based SIB needs systematic investigations toward solid-electrolyte interphase design [121] to ensure a stable and efficient interface. PVD, PECVD, and atmospheric plasma deposition of carbon have an established history for LIB and significant preliminary studies have already reported for SIB. The carbon atomic arrangement and nanoarchitecture significantly influence the performance of energy devices [122,123]. Therefore, there is a need to systematically explore the potential of PVD, PECVD, and atmospheric plasma deposition to understand the structural-property relationship for hard carbon anodes for SIB applications. Advanced techniques such as magnetic resonance imaging (MRI), neutron, nano and micro X-ray [124] are being used to understand structure of battery materials. Sodiation mechanisms in hard carbon are investigated with X-ray [125]. Hence utilization of MRI and neutron scattering could have the potential to reveal scientific mechanisms and to support in developing a structure-property relationship. Further, there is a wide gap in the implementation of computational tools and digital manufacturing approaches to make hard carbon anodes for SIB using plasma techniques. Commercial digital twin tools on plasma deposition have emerged in recent years which may be combined with machine learning tools to optimize deposition conditions, and structural-property relationship hard carbon to make high-performance anodes for SIB. There are numerous triggers such as heat, magnetic and electric fields, and chemical and mechanistic stress which influence atomic-scale chemical dynamics [126]. Hence, there is a need to develop next-generation real-time monitoring and diagnostic tools [127,128] to ensure SIB safety and long life.

The oncoming challenges are also associated with structure-property relationships by developing multi-material doping and multi-layered anode designs and electrolyte interfaces to uplift capacities and overall performance, and innovating next-generation digital tools for monitoring, diagnosing, and self-repairing of high-performance long-life sodium-based batteries. Fig. 11 presents the proposed framework for
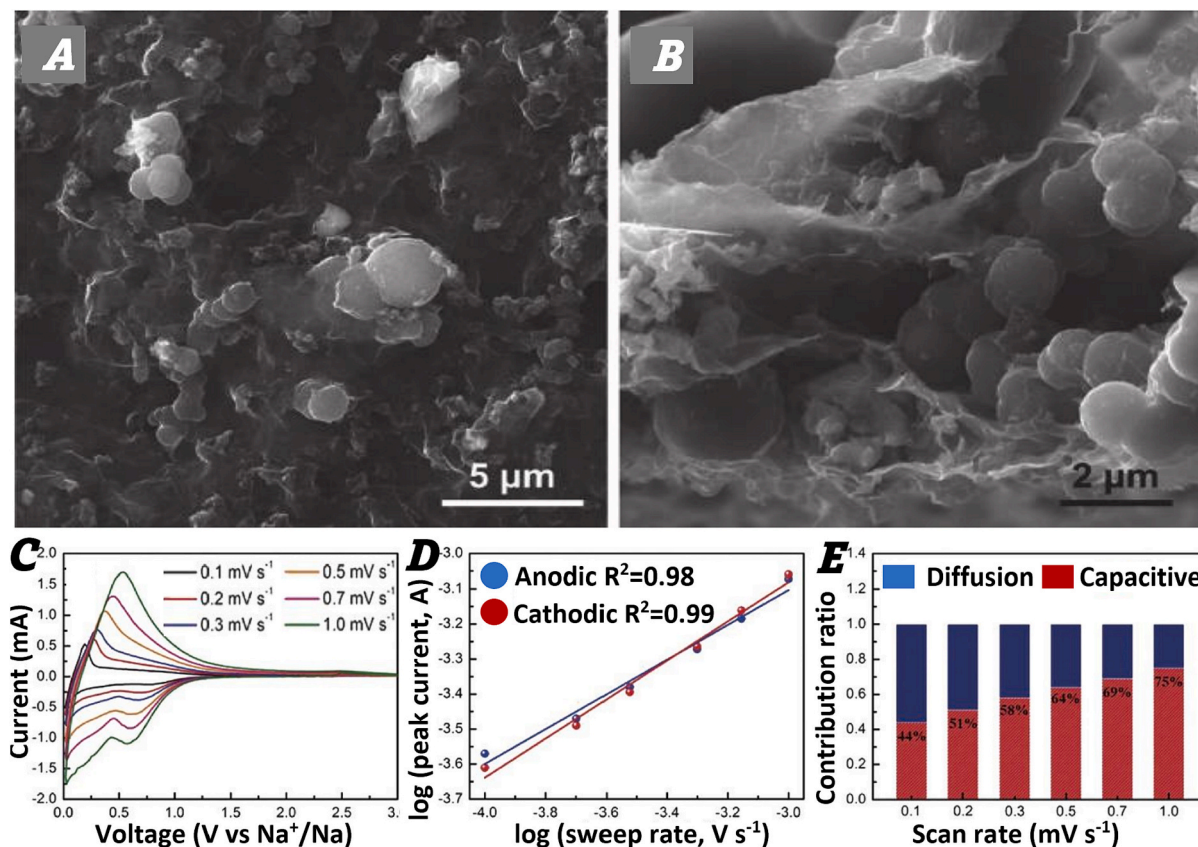
Fig. 10. Micrographs of MXene and Hard Carbon for Sodium-Ion Battery from (A) Plane and (B) Cross-sectional view after 100 cycles. (C) Cyclic-Voltammetry curves, (D) Peak current and Sweep rate, and (E) diffusion/capacitive contributions as a function of scan rates show the performance of MXene/hard carbon. Reproduced with permissions: Copyright 2022, Elsevier [105].
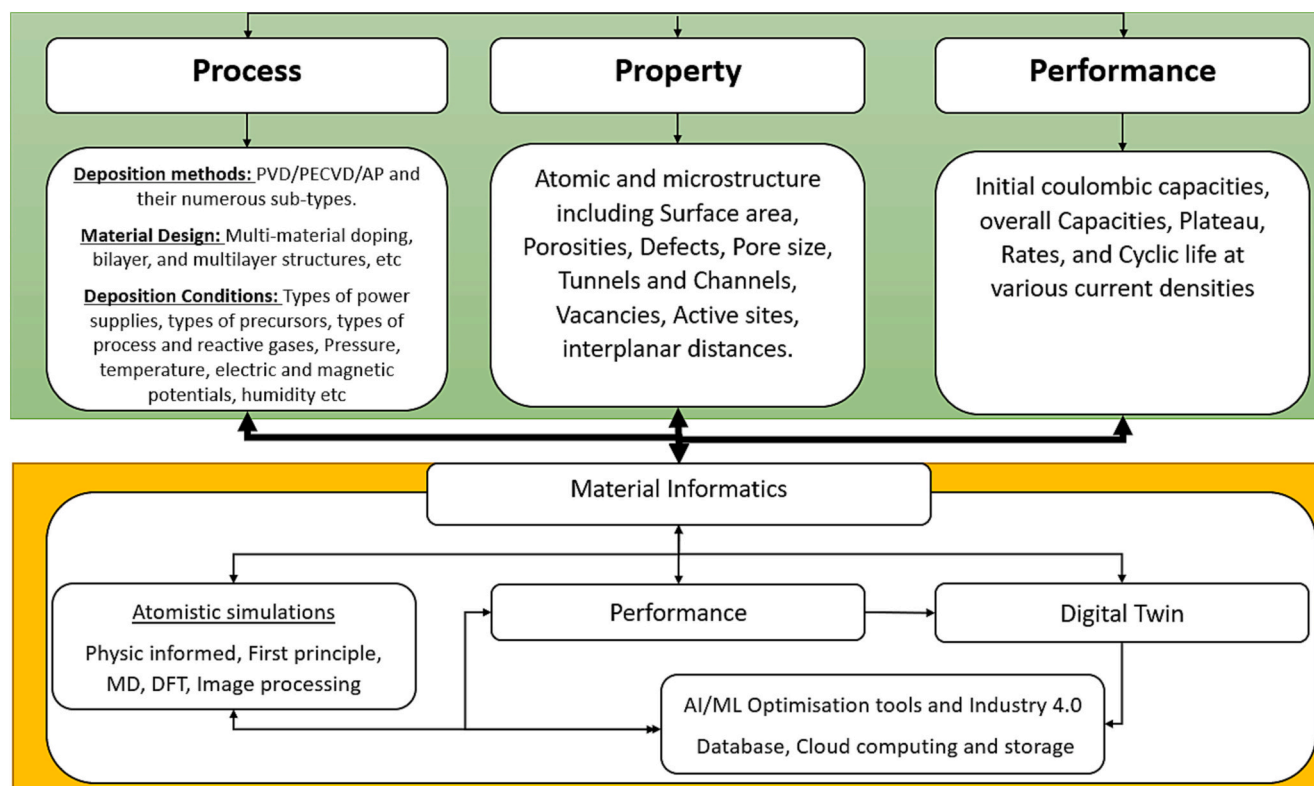
plasma-derived hard carbon for sodium-ion battery applications. The evolution phase starts with developing process-property-performance relationships. Systematic investigations are required considering the numerous indices of plasma processing methods by technology, material design, deposition conditions, and post-deposition treatments of hard carbon, that correspond to atomic and microstructures produced with a variety of porosities, interplanar spacings, defects, active sites, and regulate sodium-ion battery performance on the basis of capacities, rates, and cyclic life etc. The plasma processing of hard carbon for sodium-ion batteries may have more than 100 combinations for each plasma processing method. Therefore, experimental synthesis and in-situ measurements need to be blended with material informatics. Atomistic simulations, virtual synthesis, and machine learning [41] based optimization models are emerging for hard carbon to suggest unique structure-property relations for high-performance sodium batteries. Similarly, creating digital twins [129] of plasma-based manufacturing processes for real-time monitoring and control over the synthesis process is desirable to make superior energy storage batteries with minimal cost and resources.

In summary, plasma-derived hard carbon have proven their potential for sodium batteries, however, warrant a detailed and systematic understanding of process-property-performance relationships to unleash their full potential for sodium batteries. Plasma processing is a high-potential candidate as a scalable and sustainable method to meet the rising demands of hard carbon for energy storage applications. Plasma processing is perceived as an expensive technology, which may raise concerns over expensive hard carbon for lower-capacity SIB. The

plasma-driven hard carbon will be applicable for a range of energy storage systems as hard carbon is trending for many post-lithium batteries. Plasma processing is enough established to coat tiny articles to a few meters' large panels in a one-step process. Hence, it is capable of deposit hard carbon on large batches and roll-to-roll deposition to reduce the cost per unit article. Further, the application of plasma processing can also contribute to balancing the demand and supply of critical materials for energy storage products.

7. Conclusions

This review article briefly introduces hard carbon and its current standing for SIB. The mechanism and structural models of hard carbon from Franklin (1951) to fresh atomistic simulations are discussed. The potential role of ongoing material informatics drive in promoting hard carbon research is highlighted. The carbon atomic structure, sp^2 and sp^3 variations, significance of aromatic rings, chain structures, and atomic disorder of plasma-driven carbon and their relevance with SIB are discussed. Further, mechanisms of core plasma manufacturing techniques, such as PVD, PECVD, and atmospheric plasma deposition methods, and the influence of their operational parameters in the context of SIB are described. Plasma processing has been shown to uplift Coulombic efficiency by 33 % and specific capacity by 44 %, respectively. Particularly, spark sintering plasma has shown initial Coulombic efficiency of ~90 % reversible capacity of ~300 mAh/g and rate capacity of 136.6 mAh/g at 5 A/g. The last section describes the future aspects of plasma methods to perform multi-material doping, in-situ nanoarchitecture fabrications,

Fig. 11. Proposed framework of hard carbon for sodium-ion batteries. The typical process-property-performance relationships may have more than 100 combinations for each plasma processing method. Therefore, it is important to co-investigate experimental studies in conjunction with material informatics.

and challenges around SIB functioning in extreme environments, and the development of real-time robust monitoring and diagnostic tools to make safe, stable, and high-performance SIB with long life. Further, a data-driven manufacturing framework is proposed by integrating material informatics with experimental protocols for virtual synthesis of hard carbon; estimating material formulations, manufacturing methods, process-property-performance relationship, and limitations before physical manufacturing of high-performance sodium batteries.

CRediT authorship contribution statement

Abdul Wasy Zia: Writing – review & editing, Writing – original draft, Data curation, Conceptualization. **Shahid Rasul:** Writing – review & editing, Writing – original draft. **Muhammad Asim:** Writing – review & editing, Writing – original draft, Data curation. **Yarjan Abdul Samad:** Writing – review & editing, Writing – original draft. **Rana Abdul Shakoor:** Writing – review & editing, Writing – original draft. **Tariq Masood:** Writing – review & editing, Writing – original draft.

Declaration of competing interest

The authors declare no competing interests.

Data availability

All data regarding this publication is presented within this article.

References

[1] A. Rudola, R. Sayers, C.J. Wright, J. Barker, Opportunities for moderate-range electric vehicles using sustainable sodium-ion batteries, Nat. Energy 8 (2023) 215–218.

[2] C. del Mar Saavedra Rios, A. Beda, L. Simonin, C. Matei Ghimbeu, Hard Carbon for Na-ion Batteries: From Synthesis to Performance and Storage Mechanism, Na-ion Batteries, 2021, pp. 101–146.

[3] M. Liu, Y. Wang, F. Wu, Y. Bai, Y. Li, Y. Gong, X. Feng, Y. Li, X. Wang, C. Wu, Advances in carbon materials for sodium and potassium storage, Adv. Funct. Mater. 32 (2022) 2203117.

[4] D.A. Stevens, J.R. Dahn, High capacity anode materials for rechargeable sodium-ion batteries, J. Electrochem. Soc. 147 (2000) 1271.

[5] D. Chao, W. Zhou, F. Xie, C. Ye, H. Li, M. Jaroniec, S.-Z. Qiao, n.d. Roadmap for advanced aqueous batteries: from design of materials to applications, Science Advances, 6 eaba4098.

[6] Y. Liu, X. Hu, J. Li, G. Zhong, J. Yuan, H. Zhan, Y. Tang, Z. Wen, Carbon-coated MoS1.5Te0.5 nanocables for efficient sodium-ion storage in non-aqueous dual-ion batteries, Nat. Commun. 13 (2022) 663.

[7] R.E. Franklin, J.T. Randall, Crystallite growth in graphitizing and non-graphitizing carbons, Proc. R. Soc. A: Math. Phys. Eng. Sci. 209 (1997) 196–218.

[8] F. Xie, Z. Xu, Z. Guo, M.-M. Titirici, Hard carbons for sodium-ion batteries and beyond, Prog. Energy 2 (2020) 042002.

[9] M. Bielewski, A. Pfrang, S. Bobba, A. Kronberga, A. Georgakaki, S. Letout, A. Kuokkanen, A. Mountraki, E. Ince, D. Shtjefni, Clean Energy Technology Observatory: Batteries for Energy Storage in the European Union–2022 Status Report on Technology Development, Trends, Value Chains and Markets n.d.

[10] M. Thompson, Q. Xia, Z. Hu, X.S. Zhao, A review on biomass-derived hard carbon materials for sodium-ion batteries, Mater. Adv. 2 (2021) 5881–5905.

[11] L. Liu, Y. Tian, A. Abdussalam, M.R. Gilani, W. Zhang, G. Xu, Hard carbons as anodes in sodium-ion batteries: sodium storage mechanism and optimization strategies, Molecules 27 (19) (2022) 6516.

[12] H. Moon, A. Innocenti, H. Liu, H. Zhang, M. Weil, M. Zarrabeitia, S. Passerini, Bio-waste-derived hard carbon anodes through a sustainable and cost-effective synthesis process for sodium-ion batteries, ChemSusChem 16 (2023) e202201713.

[13] W. Shao, H. Shi, X. Jian, Z.-S. Wu, F. Hu, Hard-carbon anodes for sodium-ion batteries: recent status and challenging perspectives, Adv. Energy Sustain. Res. 3 (2022) 2200009.

[14] D. Alvira, D. Antorán, J.J. Manyà, Plant-derived hard carbon as anode for sodium-ion batteries: a comprehensive review to guide interdisciplinary research, Chem. Eng. J. 447 (2022) 137468.

[15] V. Simone, A. Boulineau, A. de Geyer, D. Rouchon, L. Simonin, S. Martinet, Hard carbon derived from cellulose as anode for sodium ion batteries: dependence of electrochemical properties on structure, J. Energy Chem. 25 (2016) 761–768.

[16] M. Lu, Y. Huang, C. Chen, Cedarwood bark-derived hard carbon as an anode for high-performance sodium-ion batteries, Energy Fuel 34 (2020) 11489–11497.

[17] P. Verma, S. Puravankara, Jute-fiber precursor-derived low-cost sustainable hard carbon with varying micro/mesoporosity and distinct storage mechanisms for sodium-ion and potassium-ion batteries, Langmuir 38 (2022) 15703–15713.

[18] E. Gibertini, F. Liberale, C. Dossi, G. Binda, B. Mattioli, R. Bettinetti, A. Maspero, M. Fiore, R. Ruffo, L. Magagnin, Algae-derived hard carbon anodes for Na-ion batteries, J. Appl. Electrochem. 51 (2021) 1665–1673.

[19] J. Choi, M.E. Lee, S. Lee, H.-J. Jin, Y.S. Yun, Pyroprotein-derived hard carbon fibers exhibiting exceptionally high plateau capacities for sodium ion batteries, ACS Appl. Energy Mater. 2 (2019) 1185–1191.

[20] B. Zhang, C.M. Ghimbeu, C. Laberty, C. Vix-Guterl, J.-M. Tarascon, Correlation between microstructure and Na storage behavior in hard carbon, Adv. Energy Mater. 6 (2016) 1501588.

[21] Z. Li, Y. Chen, Z. Jian, H. Jiang, J.J. Razink, W.F. Stickle, J.C. Neuefeind, X. Ji, Defective hard carbon anode for Na-ion batteries, Chem. Mater. 30 (2018) 4536–4542.

[22] Y. Zhen, Y. Chen, F. Li, Z. Guo, Z. Hong, M.-M. Titirici, Ultrafast synthesis of hard carbon anodes for sodium-ion batteries, Proc. Natl. Acad. Sci. 118 (2021) e2111119118.

[23] Y. Wan, Y. Liu, D. Chao, W. Li, D. Zhao, Recent advances in hard carbon anodes with high initial Coulombic efficiency for sodium-ion batteries, Nano Mater. Sci. 5 (2) (2023) 189–201.

[24] X. Chen, C. Liu, Y. Fang, X. Ai, F. Zhong, H. Yang, Y. Cao, Understanding of the sodium storage mechanism in hard carbon anodes, Carbon Energy 4 (2022) 1133–1150.

[25] N. Sun, Z. Guan, Y. Liu, Y. Cao, Q. Zhu, H. Liu, Z. Wang, P. Zhang, B. Xu, Extended "adsorption–insertion" model: a new insight into the sodium storage mechanism of hard carbons, Adv. Energy Mater. 9 (2019) 1901351.

[26] R.E. Franklin, Crystallite growth in graphitizing and non-graphitizing carbons, Proc. R. Soc. A: Math. Phys. Eng. Sci. 209 (1951) 196–218.

[27] J.H. Shinn, From coal to single-stage and two-stage products: a reactive model of coal structure, Fuel 63 (1984) 1187–1196.

[28] X. Dou, I. Hasa, D. Saurel, C. Vaalma, L. Wu, D. Buchholz, D. Bresser, S. Komaba, S. Passerini, Hard carbons for sodium-ion batteries: structure, analysis, sustainability, and electrochemistry, Mater. Today 23 (2019) 87–104.

[29] L.L. Ban, D. Crawford, H. Marsh, Lattice-resolution electron microscopy in structural studies of non-graphitizing carbons from polyvinylidene chloride (PVDC), J. Appl. Crystallogr. 8 (1975) 415–420.

[30] S.J. Townsend, T.J. Lenosky, D.A. Muller, C.S. Nichols, V. Elser, Negatively curved graphitic sheet model of amorphous carbon, Phys. Rev. Lett. 69 (1992) 921–924.

[31] P.J.F. Harris, S.C. Tsang, High-resolution electron microscopy studies of non-graphitizing carbons, Philos. Mag. A 76 (1997) 667–677.

[32] A.P. Terzyk, S. Furmaniak, P.J.F. Harris, P.A. Gauden, J. Włoch, P. Kowalczyk, G. Rychlicki, How realistic is the pore size distribution calculated from adsorption isotherms if activated carbon is composed of fullerene-like fragments? Phys. Chem. Chem. Phys. 9 (2007) 5919–5927.

[33] L. Li, W. Song, A. Ovcharenko, M. Xu, G. Zhang, Effects of atomic structure on the frictional properties of amorphous carbon coatings, Surf. Coat. Technol. 263 (2015) 8–14.

[34] X. Chen, Y. Zheng, W. Liu, C. Zhang, S. Li, J. Li, High-performance sodium-ion batteries with a hard carbon anode: transition from the half-cell to full-cell perspective, Nanoscale 11 (2019) 22196–22205.

[35] K. Chayambuka, G. Mulder, D.L. Danilov, P.H.L. Notten, Physics-based modeling of sodium-ion batteries part II, Model and validation, Electrochim. Acta 404 (2022) 139764.

[36] C. Ryu, J.-S. Kim, S.-B. Rim, S.-H. Choe, C.-J. Yu, First-principles study of ethylene carbonate adsorption on prismatic hard carbon surface: an insight into solid-electrolyte interphase formation, Appl. Surf. Sci. 573 (2022) 151495.

[37] C. Ryu, S.-B. Rim, Y. Kang, C.-J. Yu, First-principles study of sodium adsorption on defective graphene under propylene carbonate electrolyte conditions, RSC Adv. 13 (2023) 5627–5633.

[38] J. Li, T. Li, C. Peng, J. Li, H. Zhang, Molecular structure evaluation and image-guided atomistic representation of hard carbon electrodes, J. Electrochem. Soc. 169 (2022) 070517.

[39] J. Li, H. Ouyang, J. Wang, J. Li, H. Zhang, Nanostructure quantification of hard carbon electrodes through advanced HRTEM image analysis, J. Electrochem. Soc. 169 (2022) 090522.

[40] V.L. Deringer, C. Merlet, Y. Hu, T.H. Lee, J.A. Kattirtzi, O. Pecher, G. Csányi, S. R. Elliott, C.P. Grey, Towards an atomistic understanding of disordered carbon electrode materials, Chem. Commun. 54 (2018) 5988–5991.

[41] X. Liu, T. Wang, T. Ji, H. Wang, H. Liu, J. Li, D. Chao, Using machine learning to screen non-graphite carbon materials based on Na-ion storage properties, J. Mater. Chem. A 10 (2022) 8031–8046.

[42] L.-R. Cheng, Z.-Z. Lin, X.-M. Li, X. Chen, Can T-carbon serve as a Li storage material and a Li battery anode?, materials, Advances 2 (2021) 4694–4701.

[43] A. Giri, C.J. Dionne, P.E., Hopkins, atomic coordination dictates vibrational characteristics and thermal conductivity in amorphous carbon, npj Comput. Mater. 8 (2022) 55.

[44] N.A. Marks, Thin film deposition of tetrahedral amorphous carbon: a molecular dynamics study, Diam. Relat. Mater. 14 (2005) 1223–1231.

[45] M. Zawischa, S. Makowski, T. Krülle, V. Weihnacht, Structural changes of doped ta-C coatings at elevated temperature, Carbon 118182 (2023).

[46] T.W. Surta, E. Koh, Z. Li, D.B. Fast, X. Ji, P.A. Greaney, M.R. Dolgos, Combining experimental and theoretical techniques to gain an atomic level understanding of the defect binding mechanism in hard carbon anodes for sodium ion batteries, Adv. Energy Mater. 12 (2022) 2200647.

[47] T. Or, S.W.D. Gourley, K. Kaliyappan, Y. Zheng, M. Li, Z. Chen, Recent Progress in surface coatings for sodium-ion battery electrode materials, Electrochem. Energy Rev. 5 (2022) 20.

[48] Y. Oka, T. Obata, Y. Nishimura, T. Nakamura, High-temperature cycling performance of LiNi1/3Co1/3Mn1/3O2 cathode with DLC protective film, J. Electrochem. Soc. 162 (2015) A3032.

[49] S.-O. Kim, H.-T. Shim, J.K. Lee, Electrochemical performance of silicon thin film anodes covered by diamond-like carbon with various surface coating morphologies, J. Solid State Electrochem. 14 (2010) 1247–1253.

[50] Y. Zhen, Y. Chen, F. Li, Z. Guo, Z. Hong, M.-M. Titirici, Ultrafast synthesis of hard carbon anodes for sodium-ion batteries, Proc. Natl. Acad. Sci. 118 (2021).

[51] C. Donnet, A. Erdemir, Tribology of Diamond-like Carbon Films: Fundamentals and Applications, Springer Science & Business Media2007.

[52] J. Carey, S. Silva, Nanostructured materials for field emission devices, book carbon nanomaterials, Ed. Gogotsi Yu (2006) 275–294.

[53] A.C. Ferrari, S.E. Rodil, J. Robertson, Interpretation of infrared and Raman spectra of amorphous carbon nitrides, Phys. Rev. B 67 (2003) 155306.

[54] H. Ito, K. Yamamoto, Mechanical and tribological properties of DLC films for sliding parts, Kobelco, Technol. Rev. 35 (2017) 55–60.

[55] N. Ohtake, M. Hiratsuka, K. Kanda, H. Akasaka, M. Tsujioka, K. Hirakuri, A. Hirata, T. Ohana, H. Inaba, M. Kano, H. Saitoh, Properties and classification of diamond-like carbon films, Materials 14 (2) (2021) 315.

[56] W.G. Cui, Q.B. Lai, L. Zhang, F.M. Wang, Quantitative measurements of sp3 content in DLC films with Raman spectroscopy, Surf. Coat. Technol. 205 (2010) 1995–1999.

[57] A. Erdemir, C. Donnet, Tribology of diamond-like carbon films: recent progress and future prospects, J. Phys. D. Appl. Phys. 39 (2006) R311.

[58] A. Erdemir, O. Eryilmaz, Achieving superlubricity in DLC films by controlling bulk, surface, and tribochemistry, Friction 2 (2014) 140–155.

[59] C.-T. Toh, H. Zhang, J. Lin, A.S. Mayorov, Y.-P. Wang, C.M. Orofeo, D.B. Ferry, H. Andersen, N. Kakenov, Z. Guo, I.H. Abidi, H. Sims, K. Suenaga, S.T. Pantelides, B. Özyilmaz, Synthesis and properties of free-standing monolayer amorphous carbon, Nature 577 (2020) 199–203.

[60] M.I.D.B. Bouchet, C. Matta, L.-M. Th, J.M. Martin, Q. Zhang, I.W. Goddard, M. Kano, Y. Mabuchi, J. Ye, Superlubricity mechanism of diamond-like carbon with glycerol. Coupling of experimental and simulation studies, J. Phys. Conf. Ser. 89 (2007) 012003.

[61] J. Robertson, Classification of Diamond-like Carbons, Fundamentals and Applications, Tribology of Diamond-Like Carbon Films, 2008, pp. 13–24.

[62] H. Hofsäss, H. Feldermann, R. Merk, M. Sebastian, C. Ronning, Cylindrical spike model for the formation of diamondlike thin films by ion deposition, Appl. Phys. A 66 (1998) 153–181.

[63] A.W. Zia, S.A. Hussain, M.M.F.A. Baig, Optimizing diamond-like carbon coatings - From experimental era to artificial intelligence, Ceram. Int. 48 (2022) 36000–36011.

[64] A.W. Zia, M. Birkett, M.A. Badshah, M. Iqbal, Progress in-situ synthesis of graphitic carbon nanoparticles with physical vapour deposition, Prog. Cryst. Growth Charact. Mater. 67 (2021) 100534.

[65] Y. Zhang, X. Liu, W. Bai, H. Tang, S. Shi, X. Wang, C. Gu, J. Tu, Magnetron sputtering amorphous carbon coatings on metallic lithium: towards promising anodes for lithium secondary batteries, J. Power Sources 266 (2014) 43–50.

[66] S. Javeed, S. Yamin, S.A. Janjua, K. Yaqub, A. Ashraf, S. Zeeshan, M. Mehmood, M. Anwar-Ul-Haq, S. Ahmad, Amorphous carbon films in direct current magnetron sputtering from regenerative sooting discharge, Vacuum 86 (2011) 193–200.

[67] J. Matlak, K. Komvopoulos, Friction properties of amorphous carbon ultrathin films deposited by filtered cathodic vacuum arc and radio-frequency sputtering, Thin Solid Films 579 (2015) 167–173.

[68] P. Vašina, P. Souček, T. Schmidtová, M. Eliáš, V. Buršíková, M. Jílek, M. Jílek Jr., J. Schäfer, J. Buršík, Depth profile analyses of nc-TiC/aC: H coating prepared by balanced magnetron sputtering, Surf. Coat. Technol. 205 (2011) S53–S56.

[69] D. Monaghan, D. Teer, P. Logan, I. Efeoglu, R. Arnell, Deposition of wear resistant coatings based on diamond like carbon by unbalanced magnetron sputtering, Surf. Coat. Technol. 60 (1993) 525–530.

[70] H. Fukue, T. Nakatani, T. Okano, M. Kuroiwa, S. Kunitsugu, H. Oota, K. Yonezawa, Effect of tail time of discharge current on film properties in diamond-like carbon deposition by high-frequency inclusion high-power impulse magnetron sputtering, Diam. Relat. Mater. 135 (2023) 109868.

[71] K. Zdunek, R. Chodun, B. Wicher, K. Nowakowska-Langier, S. Okrasa, Characterization of sp3 bond content of carbon films deposited by high power gas injection magnetron sputtering method by UV and VIS Raman spectroscopy, Spectrochim. Acta A Mol. Biomol. Spectrosc. 194 (2018) 136–140.

[72] J. Zhu, J. Han, X. Han, H.I. Schlaberg, J. Wang, sp3-rich deposition conditions and growth mechanism of tetrahedral amorphous carbon films deposited using filtered arc, J. Appl. Phys. 104 (2008) 013512.

[73] M.I. De Barros Bouchet, J.M. Martin, J. Avila, M. Kano, K. Yoshida, T. Tsuruda, S. Bai, Y. Higuchi, N. Ozawa, M. Kubo, M.C. Asensio, Diamond-like carbon coating under oleic acid lubrication: evidence for graphene oxide formation in superlow friction, Sci. Rep. 7 (2017) 46394.

[74] P.J. Fallon, V.S. Veerasamy, C.A. Davis, J. Robertson, G.A.J. Amaratunga, W. I. Milne, J. Koskinen, Properties of filtered-ion-beam-deposited diamondlike carbon as a function of ion energy, Phys. Rev. B 48 (1993) 4777–4782.

[75] J. Koskinen, A. Anttila, J.-P. Hirvonen, Diamond-like carbon coatings by arc-discharge methods, Surf. Coat. Technol. 47 (1991) 180–187.

[76] J.-I. Kim, Y.-J. Jang, J. Kim, J. Kim, Effects of silicon doping on low-friction and high-hardness diamond-like carbon coating via filtered cathodic vacuum arc deposition, Sci. Rep. 11 (2021) 1–13.

[77] F.M. Kimock, B.J. Knapp, Commercial applications of ion beam deposited diamond-like carbon (DLC) coatings, Surf. Coat. Technol. 56 (1993) 273–279.

[78] S. Rabadzhiyska, G. Kotlarski, M. Shipochka, P. Rafailov, M. Ormanova, V. Strijkova, N. Dimcheva, S. Valkov, Duplex surface modification of 304-L SS substrates by an electron-beam treatment and subsequent deposition of diamond-like carbon coatings, Coatings 12 (2022) 401.

[79] A. Voevodin, M. Donley, J. Zabinski, Pulsed laser deposition of diamond-like carbon wear protective coatings: a review, Surf. Coat. Technol. 92 (1997) 42–49.

[80] J. Solis, H. Zhao, C. Wang, J. Verduzco, A. Bueno, A. Neville, Tribological performance of an H-DLC coating prepared by PECVD, Appl. Surf. Sci. 383 (2016) 222–232.

[81] J. Robertson, Diamond-like amorphous carbon, Mater. Sci. Eng. R Rep. 37 (2002) 129–281.

[82] J. Robertson, The deposition mechanism of diamond-like a-C and a-C: H, Diam. Relat. Mater. 3 (1994) 361–368.

[83] O. Godoy-Cabrera, R. López-Callejas, R. Valencia, A. Muñoz-Castro, S.R. Barocio, E. Chávez A, A. Mercado-Cabrera, A. de la Piedad-Beneitez, B. Rodríguez-Méndez, J. Rodríguez-Arce, Effect of air-oxygen and argon-oxygen mixtures on dielectric barrier discharge decomposition of toluene, Braz. J. Phys. 34 (2004).

[84] R. Pothiraja, N. Bibinov, P. Awakowicz, Amorphous carbon film deposition on the inner surface of tubes using atmospheric pressure pulsed filamentary plasma source, J. Phys. D. Appl. Phys. 44 (2011) 355206.

[85] T. Suzuki, A. Shirakura, Synthesis of diamond-like hydrocarbon films by atmospheric pressure filamentary dielectric barrier discharge, in: IOP Conference Series: Materials Science and Engineering, IOP Publishing, 2018, p. 012046.

[86] A. Habibi, S.M. Khoie, F. Mahboubi, M. Urgen, Raman spectroscopy of thin DLC film deposited by plasma electrolysis process, Surf. Coat. Technol. 309 (2017) 945–950.

[87] C. Fei, J.Q. Chen, H. Zhou, C.M. Li, DLC Films Synthesized on the Ti6Al4V Alloy Surface by Plasma Gun at an Atmospheric Pressure, Trans Tech Publ, Materials Science Forum, 2011, pp. 739–744.

[88] A. Abbass, S. Kadhem, Preparation and characterization DLC thin films using atmospheric pressure plasma jet, in: IOP Conference Series: Materials Science and Engineering, IOP Publishing, 2018, p. 012065.

[89] H. Thejaswini, A.R. Hoskinson, B. Agasanapura, M. Grunde, J. Hopwood, Deposition and characterization of diamond-like carbon films by microwave resonator microplasma at one atmosphere, Diam. Relat. Mater. 48 (2014) 24–31.

[90] R.M. Pujahari, Chapter 2- Solar cell technology, in: S.J. Dhoble, N.T. Kalyani, B. Vengadaesvaran, A. Kariem Arof (Eds.) Energy Materials, Elsevier2021, pp. 27–60.

[91] A. Anders, Cathodic arc technology, in: Q.J. Wang, Y.-W. Chung (Eds.), Encyclopedia of Tribology, Springer, US, Boston, MA, 2013, pp. 311–318.

[92] S.N. Ogugua, O.M. Ntwaeaborwa, H.C. Swart, Latest development on pulsed laser deposited thin films for advanced luminescence applications, Coatings 10 (11) (2020) 1078.

[93] Z. Ju, J. Lin, S. Shen, B. Wu, E. Wu, Preparations and applications of single color centers in diamond, Adv. Phys. X 6 (2021) 1858721.

[94] K.Y. Perera, J. Prendeville, A.K. Jaiswal, S. Jaiswal, Cold plasma Technology in Food Packaging, Coatings 12 (12) (2022) 1896.

[95] J. Robertson, Properties of diamond-like carbon, Surf. Coat. Technol. 50 (1992) 185–203.

[96] J. Robertson, Hard amorphous (diamond-like) carbons, Prog. Solid State Chem. 21 (1991) 199–333.

[97] H. Xie, Z. Wu, Z. Wang, N. Qin, Y. Li, Y. Cao, Z. Lu, Solid electrolyte interface stabilization via surface oxygen species functionalization in hard carbon for superior performance sodium-ion batteries, J. Mater. Chem. A 8 (2020) 3606–3612.

[98] W. Zhang, Y. Liu, Z. Guo, Approaching high-performance potassium-ion batteries via advanced design strategies and engineering, Science Advances, 5 eaav7412.

[99] C. Shen, C. Wang, T. Jin, X. Zhang, L. Jiao, K. Xie, Tailoring the surface chemistry of hard carbon towards high-efficiency sodium ion storage, Nanoscale 14 (2022) 8959–8966.

[100] X. Wu, S. Wu, C. Wu, X. Zhang, Z. Jiang, S. Liu, N. Li, Plasma-promoted surface regulation of a novel integrative carbon network for boosting the long-cycle capability of sodium-ion storage, Carbon 191 (2022) 112–121.

[101] Q. Sun, Y. Yang, Z.-W. Fu, Electrochemical properties of room temperature sodium–air batteries with non-aqueous electrolyte, Electrochem. Commun. 16 (2012) 22–25.

[102] J. Wu, S. Moradmand, W.K. Pang, J. Allen, N. Sharma, Sodium-ion battery anodes from carbon depositions, Electrochim. Acta 379 (2021) 138109.

[103] D.-Y. Kim, O.L. Li, J. Kang, Novel synthesis of highly phosphorus-doped carbon as an ultrahigh-rate anode for sodium ion batteries, Carbon 168 (2020) 448–457.

[104] H.-S. Yang, M.-W. Park, K.-H. Kim, O.L. Li, T.-I. Jeon, J. Kang, Facile in situ synthesis of dual-heteroatom-doped high-rate capability carbon anode for rechargeable seawater-batteries, Carbon 189 (2022) 251–264.

[105] H.-l. Cao, L.-t. Yang, M. Zhao, P.-z. Liu, C.-l. Guo, B.-s. Xu, J.-j. Guo, A flexible hard carbon microsphere/MXene film as a high-performance anode for sodium-ion storage, New Carbon Mater., 37 (2022) 1154–1160.

[106] M. Zarrabeitia, F. Nobili, O. Lakuntza, J. Carrasco, T. Rojo, M. Casas-Cabanas, M.Á. Muñoz-Márquez, Role of the voltage window on the capacity retention of P2-Na2/3[Fe1/2Mn1/2]O2 cathode material for rechargeable sodium-ion batteries, Commun. Chem. 5 (2022) 11.

[107] R. Usiskin, Y. Lu, J. Popovic, M. Law, P. Balaya, Y.-S. Hu, J. Maier, Fundamentals, status and promise of sodium-based batteries, Nat. Rev. Mater. 6 (2021) 1020–1035.

[108] Q. Liu, R. Xu, D. Mu, G. Tan, H. Gao, N. Li, R. Chen, F. Wu, Progress in electrolyte and interface of hard carbon and graphite anode for sodium-ion battery, carbon, Energy 4 (2022) 458–479.

[109] J. Meng, G. Jia, H. Yang, M. Wang, Recent advances for SEI of hard carbon anode in sodium-ion batteries: a mini review, Front. Chem. 10 (2022).

[110] X. Qiu, X. Wang, Y. He, J. Liang, K. Liang, B.L. Tardy, J.J. Richardson, M. Hu, H. Wu, Y. Zhang, O.J. Rojas, I. Manners, J. Guo, Superstructured mesocrystals through multiple inherent molecular interactions for highly reversible sodium ion batteries, Science Advances, 7 eabh3482.

[111] Y.S. Wu, P.R. Lyu, Double-coated hard carbon as an anode material for high C-rate Lithium ion batteries, Mater. Sci. Forum 921 (2018) 105–110.

[112] X.-X. He, J.-H. Zhao, W.-H. Lai, R. Li, Z. Yang, C.-m. Xu, Y. Dai, Y. Gao, X.-H. Liu, L. Li, G. Xu, Y. Qiao, S.-L. Chou, M. Wu, Soft-carbon-coated, free-standing, low-defect, hard-carbon anode to achieve a 94% initial coulombic efficiency for sodium-ion batteries, ACS Appl. Mater. Interfaces, 13 (2021) 44358–44368.

[113] P. Zheng, T. Liu, S. Guo, Micro-nano structure hard carbon as a high performance anode material for sodium-ion batteries, Sci. Rep. 6 (2016) 35620.

[114] H. Cheng, N. Garcia-Araez, A.L. Hector, Enhancing the performance of hard carbon for sodium-ion batteries by coating with silicon nitride/oxycarbide nanoparticles, materials, Advances 2 (2021) 7956–7966.

[115] D. Ledwoch, J.B. Robinson, D. Gastol, K. Smith, P.R. Shearing, D.J.L. Brett, E. Kendrick, Hard carbon composite electrodes for sodium-ion batteries with Nano-zeolite and carbon black additives, Batteries Supercaps 4 (2021) 163–172.

[116] Z. Li, C. Bommier, Z.S. Chong, Z. Jian, T.W. Surta, X. Wang, Z. Xing, J. C. Neufeind, W.F. Stickle, M. Dolgos, P.A. Greaney, X. Ji, Mechanism of Na-ion storage in hard carbon anodes revealed by heteroatom doping, Adv. Energy Mater. 7 (2017) 1602894.

[117] Q. Shi, R. Qi, X. Feng, J. Wang, Y. Li, Z. Yao, X. Wang, Q. Li, X. Lu, J. Zhang, Y. Zhao, Niobium-doped layered cathode material for high-power and low-temperature sodium-ion batteries, Nat. Commun. 13 (2022) 3205.

[118] X. Wang, C. Zhang, M. Sawczyk, J. Sun, Q. Yuan, F. Chen, T.C. Mendes, P. C. Howlett, C. Fu, Y. Wang, X. Tan, D.J. Searles, P. Král, C.J. Hawker, A. K. Whittaker, M. Forsyth, Ultra-stable all-solid-state sodium metal batteries enabled by perfluoropolyether-based electrolytes, Nat. Mater. 21 (2022) 1057–1065.

[119] X. Wu, S. Jin, Z. Zhang, L. Jiang, L. Mu, Y.-S. Hu, H. Li, X. Chen, M. Armand, L. Chen, X. Huang, Unraveling the storage mechanism in organic carbonyl electrodes for sodium-ion batteries, Science Advances, 1 e1500330.

[120] Y. Jin, P.M.L. Le, P. Gao, Y. Xu, B. Xiao, M.H. Engelhard, X. Cao, T.D. Vo, J. Hu, L. Zhong, B.E. Matthews, R. Yi, C. Wang, X. Li, J. Liu, J.-G. Zhang, Low-solvation electrolytes for high-voltage sodium-ion batteries, nature, Energy 7 (2022) 718–725.

[121] G. Åvall, P. Adelhelm, Solution to dissolution, nature, Energy 7 (2022) 682–683.

[122] M. Kim, R. Xin, J. Earnshaw, J. Tang, J.P. Hill, A. Ashok, A.K. Nanjundan, J. Kim, C. Young, Y. Sugahara, J. Na, Y. Yamauchi, MOF-derived nanoporous carbons with diverse tunable nanoarchitectures, Nat. Protoc. 17 (2022) 2990–3027.

[123] J. Peng, D. Schwalbe-Koda, K. Akkiraju, T. Xie, L. Giordano, Y. Yu, C.J. Eom, J. R. Lunger, D.J. Zheng, R.R. Rao, S. Muy, J.C. Grossman, K. Reuter, R. Gómez-Bombarelli, Y. Shao-Horn, Human- and machine-centred designs of molecules and materials for sustainability and decarbonization, Nat. Rev. Mater. 7 (2022) 991–1009.

[124] R.F. Ziesche, T.M.M. Heenan, P. Kumari, J. Williams, W. Li, M.E. Curd, T. L. Burnett, I. Robinson, D.J.L. Brett, M.J. Ehrhardt, P.D. Quinn, L.B. Mehdi, P. J. Withers, M.M. Britton, N.D. Browning, P.R. Shearing, Multi-dimensional characterization of battery materials, Adv. Energy Mater. 13 (2023) 2300103.

[125] X. Tan, K. Jiang, S. Zhai, J. Zhou, J. Wang, K. Cadien, Z. Li, X-ray Spectromicroscopy investigation of heterogeneous Sodiation in hard carbon Nanosheets with vertically oriented (002) Planes, Small 17 (2021) 2102109.

[126] F.M. Alcorn, P.K. Jain, R.M. van der Veen, Time-resolved transmission electron microscopy for nanoscale chemical dynamics, nature reviews, Chemistry 7 (2023) 256–272.

[127] C. Gervillié-Mouravieff, C. Boussard-Plédel, J. Huang, C. Leau, L.A. Blanquer, M. B. Yahia, M.L. Doublet, S.T. Boles, X.H. Zhang, J.L. Adam, J.M. Tarascon, Unlocking cell chemistry evolution with operando fibre optic infrared spectroscopy in commercial Na(Li)-ion batteries, nature, Energy 7 (2022) 1157–1169.

[128] J. Sun, M. Sadd, P. Edenborg, H. Grönbeck, P.H. Thiesen, Z. Xia, V. Quintano, R. Qiu, A. Matic, V. Palermo, Real-time imaging of Na+ reversible intercalation in "Janus" graphene stacks for battery applications, Science Advances, 7 eabf0812.

[129] A. Pflug, S. Bruns, T. Zickenrott, C. Britze, M. Vergöhl, A digital twin for PVD deposition of tailored coatings on 3D substrates, in: R. Sargent, A. Sytchkova (Eds.) Optical Interference Coatings Conference (OIC) 2022, Optica Publishing Group, Whistler, British Columbia, 2022, pp. TC.8.